c-Myc inhibits macrophage antimycobacterial response in *Mycobacterium tuberculosis* infection

Edoardo Sarti[1¶], Cédric Dollé[1¶], Rebekka Wolfensberger[1], Katharina Kusejko[1,7], Doris Russenberger[1], Simon Bredl[1], Roberto F. Speck[1], Melanie Greter[2], Jan H. Rueschoff[3], Lucas Boeck[4], Dat Mai[5], Alan H. Diercks[5], Peter Sander[6,8], Gregory S. Olson[5,9], Johannes Nemeth[1*]

[1] Division of Infectious Diseases and Hospital Epidemiology, University Hospital Zurich, Zürich, Switzerland

[2] Institute of Experimental Immunology, University of Zurich, Zürich, Switzerland

[3] Department of Pathology and Molecular Pathology, University Hospital Zurich, Zürich, Switzerland

[4] Department of Biomedicine, University of Basel, Basel, Switzerland

[5] Center for Global Infectious Disease Research, Seattle Children's Research Institute, Seattle, Washington, United States of America

[6] Institute of Medical Microbiology, University of Zurich, Zürich, Switzerland

[7] Institute of Medical Virology, University of Zurich, Zürich, Switzerland

[8] National Reference Laboratory for Mycobacteria, University of Zurich, Zürich, Switzerland

[9] Department of Laboratory Medicine and Pathology, University of Washington, Seattle, Washington, United States of America

[¶] These authors contributed equally

[*] Corresponding author and lead contact

E-mail: johannes.nemeth@usz.ch

Abstract

Mycobacterium tuberculosis (MTB) is a major global cause of mortality worldwide, responsible for over a million deaths annually. Despite this burden, natural immunity prevents disease in more than 90% of exposed individuals. Previous studies have identified interferon-gamma (IFN-γ) as a key regulator of innate immune defense against MTB. Here, we investigate the impact of IFN-γ timing on macrophage-mediated control of MTB infection. We demonstrate that IFN-γ exposure before infection enhances macrophage antibacterial activity, whereas post-infection exposure does not. Further investigation into this phenotype revealed a strong association between c-Myc signaling and macrophage function in MTB control, as identified using unbiased *in vitro* systems approaches. Given the challenge of perturbing c-Myc in primary cells, we developed a lentiviral system for c-Myc inhibition and overexpression. Using a tetracycline-inducible Omomyc system - a small peptide inhibitor of c-Myc - we show that c-Myc inhibition promotes a pro-inflammatory macrophage phenotype with enhanced anti-mycobacterial activity. Mechanistically, c-Myc inhibition induces metabolic reprogramming via increased mTORC1 activity, leading to upregulated inducible nitric oxide synthase and improved bacterial clearance. *In vivo* analyses, including murine models and human clinical histopathology, reveal a strong correlation between c-Myc expression and MTB persistence, as well as active tuberculosis (TB), suggesting a role for c-Myc in immune evasion. These findings reveal c-Myc as a potential mediator of immune privilege in MTB infection and highlight its role as a promising target for novel TB therapies aimed at enhancing macrophage function.

Author Summary

Tuberculosis (TB), caused by *Mycobacterium tuberculosis* (MTB), remains a major global health threat. While most people exposed to MTB successfully fight off the infection, some individuals develop active disease. Understanding how the bacteria evade immune defenses is key to developing better treatments. In this study, we identify a new role for c-Myc, a protein well-known in cancer research, in suppressing the ability of immune cells called macrophages to fight MTB. Macrophages are responsible for engulfing and killing bacteria, but we found that c-Myc interferes with this process, allowing MTB to survive. Using a small peptide inhibitor called Omomyc, we were able to block c-Myc activity, which restored macrophages' ability to kill MTB. This effect is linked to changes in cellular metabolism, leading to the increased production of molecules essential for bacterial destruction. We also discovered that high c-Myc levels are associated with persistent MTB infection in both mouse models and human tissues. This suggests that c-Myc helps the bacteria evade immune attack, contributing to long-term infection. Our findings reveal a previously unknown mechanism exploited by MTB to survive in the body and suggest that targeting c-Myc could be a promising approach to enhancing immune defenses against TB. By bridging insights from cancer biology and infectious disease research, our work provides a new perspective on tackling TB and highlights c-Myc as a potential therapeutic target for boosting immunity against this deadly infection.

Introduction

Mycobacterium tuberculosis (MTB) remains the leading cause of death from a single infectious agent worldwide, responsible for approximately 1.25 million deaths annually, according to the World Health Organization (WHO)[1]. The emergence and spread of antibiotic-resistant strains of MTB demand alternative tools beyond antibiotics to achieve the objectives of global tuberculosis (TB) control efforts.

Although MTB infection is either cleared or effectively controlled by the host immune system in most cases, no host-directed therapies exist for the treatment of active TB[2]. Observations from animal models, human studies, natural infections with HIV-1, and new anti-inflammatory therapies (e.g. anti-TNF therapy) have identified pro-inflammatory macrophages and T cells to be critical components of an effective host immune response[3]. The ensuing immune response may result in profound heterogeneity in the outcomes of MTB infection[4], ranging from deadly disease to complete clearance without any sequelae[2,5,6]. This variability is observed not only across populations but also within individual infected organisms across different species, including mice, non-human primates, and humans.[6–8]

To investigate competent host immunity, we have previously focused on asymptomatic MTB infection, the most common, yet underexplored, outcome of MTB infection. Asymptomatic infection appears to confer protection against reinfection—a phenomenon observed in mouse models, non-human primates, and humans [9–11]. In our studies, mice initially received an intradermal inoculation, leading to an asymptomatic primary infection localized within the draining lymph node (contained MTB infection, CMTB). Compared to uninfected controls, mice with CMTB demonstrated a significantly faster and stronger immune response to a secondary, pulmonary challenge. This response included heightened activation of alveolar macrophages and rapid recruitment of inflammatory monocytes and T cells, driven by low-grade systemic Interferon (IFN)-γ. Consequently, these mice exhibited a substantially lower bacterial burden in the lungs than those without prior infection[9].

IFN-γ is a key cytokine in both innate and adaptive immunity, primarily produced by NK cells and CD4+ T cells[12]. Under stress or infection, IFN-γ enhances macrophage activation by increasing proinflammatory cytokines and suppressing anti-inflammatory responses, which supports both innate and adaptive

immunity[13,14]. It also boosts macrophage phagocytic and cytolytic abilities, facilitating pathogen elimination—a process termed classical macrophage activation. Additionally, IFN-γ triggers signaling cascades that upregulate genes for reactive oxygen and nitrogen species, while also influencing metabolic pathways to meet the energy demands of activated macrophages in response to external stressors, including mycobacterial infections[13].

Interestingly, in cases of active TB in humans, there are often high levels of IFN-γ present at the infection site[15,16]. This counterintuitive observation suggests that, despite the abundance of this potent pro-inflammatory cytokine, certain tissues may not be responding adequately to the IFN-γ stimulus[4]. This impaired response could indicate a form of immune resistance or dysfunction[17], where macrophages and other immune cells fail to fully activate or sustain their antimicrobial functions even in the presence of IFN-γ[2,3,18].

Based on this conundrum, the starting point for the following work was the hypothesis that the timing of IFN-γ exposure on macrophages relative to MTB infection is crucial for their effective response to MTB infection. Thus, we hypothesized that the sequence of cytokine exposure and MTB infection could significantly influence macrophage activation states and, consequently, their ability to control bacterial growth. Therefore, we decided to investigate how the timing of IFN-γ exposure—whether before or after *in vitro* infection—affects macrophage activation, gene expression, and antibacterial activity.

Results

The sequence of infection and activation determines the outcome of Mycobacterium tuberculosis infection in macrophages

We hypothesized that the timing of IFN-γ exposure are critical factors in determining infection outcomes. To test this, we conducted an *in vitro* experiment using C57BL/6 murine bone marrow-derived macrophages (BMDMs) divided into four groups. To assess bacterial growth, we used a colony-forming unit (CFU) assay, in which macrophages were lysed, and cell lysates were plated on agar to quantify viable *Mycobacterium tuberculosis* (MTB) by counting bacterial colonies.

The experimental groups included: (1) macrophages continuously exposed to IFN-γ throughout the 6-day experiment of infection with the virulent MTB strain H37Rv, including the pretreatment period, (2) macrophages pre-treated with 25 ng/mL IFN-γ starting 24 hours prior to infection, but thereafter removed, (3) macrophages treated with 25 ng/mL IFN-γ immediately post-infection (approximately 1h after phagocytosis) and maintained for 5 days, and (4) a control group with no IFN-γ treatment (Figure 1A).

Results from CFU assays revealed that only macrophages exposed to IFN-γ prior to infection, with or without continued exposure, showed improved control of MTB growth. In contrast, macrophages treated with IFN-γ post-infection did not exhibit enhanced antimycobacterial activity, as indicated by higher CFU counts. (Figure 1B + Supplementary Figure 1).

To assess both functionality and survival of phagocyted MTB, as well as the transcriptional state at the single-cell level, we utilized the MTB live-dead strain[19]. This strain expresses two fluorescent proteins, mCherry and GFP: mCherry is constitutively expressed, allowing identification of cells with phagocytosed bacteria, while GFP expression is controlled by a tetracycline-inducible promoter, enabling distinction between active ($mCherry^{+}/GFP^{+}$) and inactive ($mCherry^{+}/GFP^{-}$) MTB (Figure 1C).

While the live-dead strain has primarily been used in fluorescence microscopy[19–21], we applied it in flow cytometry. To validate this approach, we compared the live-dead strain results with CFU assays using

isoniazid-treated H37Rv, finding a comparable reduction in transcriptional activity and CFU counts (Supplementary Figure 2).

Using flow cytometry and the live-dead strain, we confirmed that macrophages exposed to IFN-γ prior to infection suppress transcriptional activity in approximately 50% of intracellular MTB. In contrast, macrophages treated with IFN-γ post-phagocytosis were unable to inhibit MTB transcriptional activity (Figure 1D).

Simultaneously, this assay allowed us to evaluate macrophage activation, with enhanced antimycobacterial activity correlating with upregulation of MHC-II and CD86 surface markers (Figures 1E-1F). These results suggest that the increased bacterial control observed in CFU assays was due to the heightened antimycobacterial function of viable BMDMs, rather than an artifact from macrophage death or extracellular bacteria.

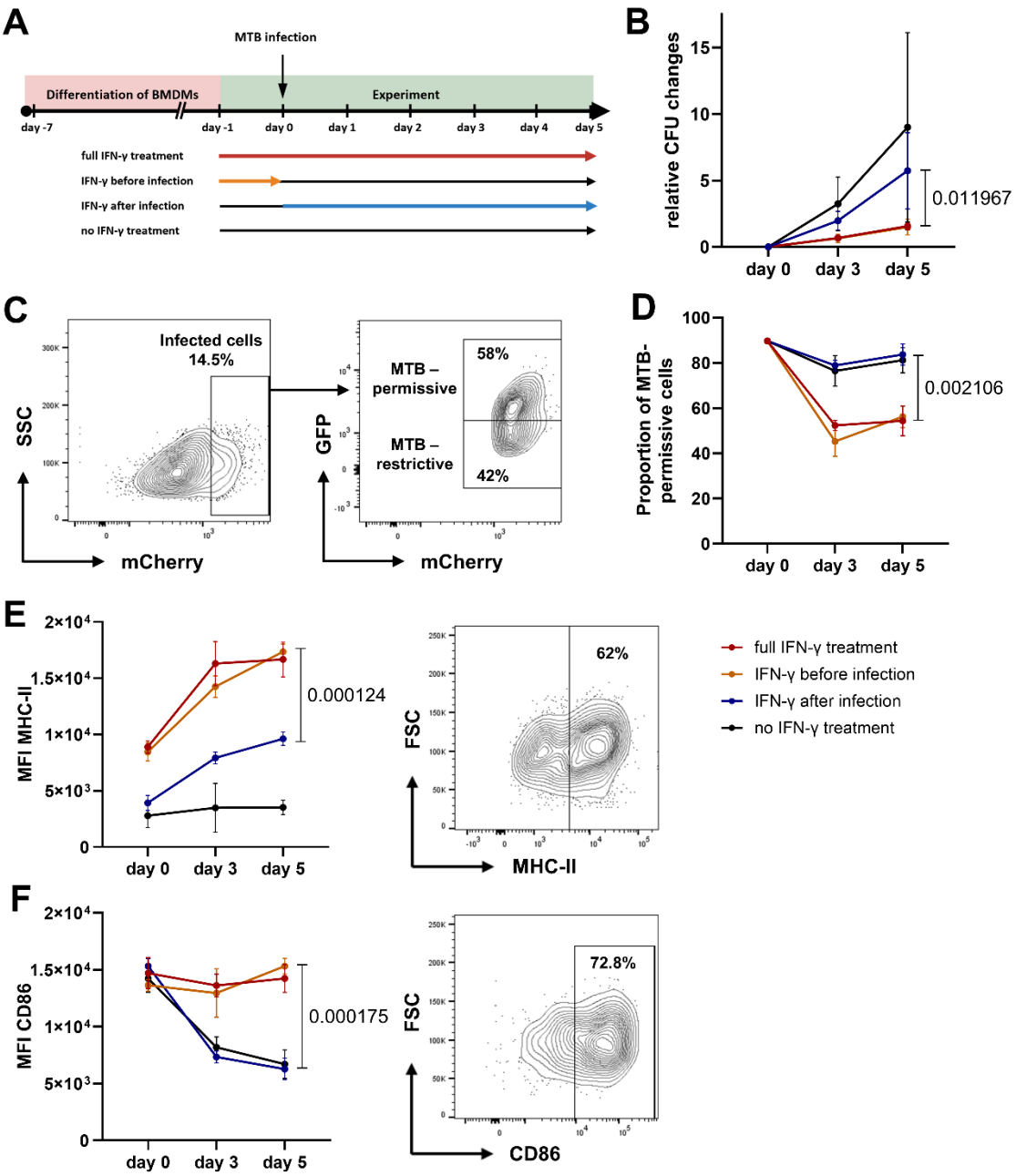

Figure 1. Antimycobacterial properties of IFN-γ depend on the sequence of infection and IFN-γ exposure

A) Experimental setup. BMDMs were obtained from C57BL/6 mice and matured for 6 days. BMDMs were then treated with IFN-γ (20ng/mL) either 24h before or directly after infection, depending on the conditions, with MTB H37Rv at a multiplicity of infection (MOI) of 5. Growth media was changed daily. **B)** Relative changes in

colony forming units per milliliter (CFU/mL) of intracellular MTB H37Rv in BMDMs activated with IFN-γ at different timepoints. Measurements were taken immediately after phagocytosis (day 0) and at 3 and 5 days post-infection. Data represent mean relative changes (range) ± standard deviation from five independent experiments. *P* values were calculated with Student's t-test between BMDMs activated with IFN-γ before and after infection. **C)** Flow cytometry gating strategy using the MTB live-dead reporter strain. Infected cells ($mCherry^+$) are further separated in permissive or restrictive based the ability of MTB to produce tetracycline-inducible GFP expression after 24h of treatment with doxycycline (synthetic tetracycline analogue) (1µg/mL). **D)** Proportion of infected macrophages containing live MTB (MTB-permissive) from the live-dead MTB reporter strain immediately after phagocytosis (day 0) at 3 and 5 days post-infection. **E-F)** Mean fluorescence intensity (MFI) of activation markers (MHC-II and CD86) in infected macrophages at day 0, 3 and 5 and representative plots (condition full treatment is shown). Data are mean ± standard deviation of 3 independent experiments. *P* values were calculated using Student's t-test.

c-Myc associated transcriptional programs mirror the *in vitro* phenotype in mature macrophages

To assess the transcriptome underlying the different infection timepoints and activation states, we conducted bulk RNA sequencing (RNA-seq) at 6 hours and 24 hours post-infection in the previously described groups of BMDMs. Principal Component Analysis (PCA) revealed that as early as 6 hours post-infection, macrophages activated prior to infection began clustering distinctly from those activated after infection (Figure 2A). Specifically, macrophages activated before infection clustered more closely with fully activated cells (MTB-controlling cells), while those activated post-infection clustered nearer to untreated cells (MTB-permissive cells). This distinction became more pronounced at 24 hours, with macrophages activated prior to infection clustering with fully activated cells, whereas those activated post-infection formed a separate cluster, distinct from both fully activated and untreated cells.

These findings indicate that by 6 hours post-infection, macrophages have already committed to a trajectory that predicts the outcome of the infection. The observation that cells receiving IFN-γ post-infection diverge

from unstimulated cells but do not cluster with cells that received IFN-γ prior to infection suggests that while these cells can respond to IFN-γ, their trajectory differs significantly from those pre-activated with IFN-γ.

At the single gene level, macrophages treated after infection and macrophages treated before infection have a clearly different expression signature, with 524 significantly upregulated genes and 627 significantly downregulated genes (Figure 2B).

We performed Gene Set Enrichment Analysis (GSEA) for functional categorization. Comparisons of gene expression profiles between macrophages activated after infection versus macrophages activated prior to infection revealed a relative downregulation of multiple pro-inflammatory pathways in cells that received IFN-γ after infection (Figure 2C). Notably, however, the most significant changes, in terms of fold changes, were not among the classical pro-inflammatory genes but were instead related to cell cycle genes, including E2F targets, G2M targets, and MYC-associated genes, which are upregulated in macrophages treated after infection.

c-Myc-associated genes were the only set of genes that fully mirrored our *in vitro* phenotype of MTB-permissive versus MTB-controlling cells. Macrophages capable of controlling MTB downregulated the leading-edge genes of the c-Myc-associated pathway (Figure 2D). In contrast, cells that received IFN-γ after infection exhibited some transcriptional response to IFN-γ (Figure 2D) but did not show any detectable increase in mycobacterial control (Figure 1). In line with the findings above, the expression of c-Myc mirror the activation of the MYC-regulated genes and is also downregulated specifically in cells capable of controlling MTB infection (Figure 2E).

These findings suggest that at the transcriptional level, the ability to downregulate c-Myc-associated transcriptional programs is strongly associated with a macrophage's capacity to mount an effective immune response that controls *in vitro* MTB infection.

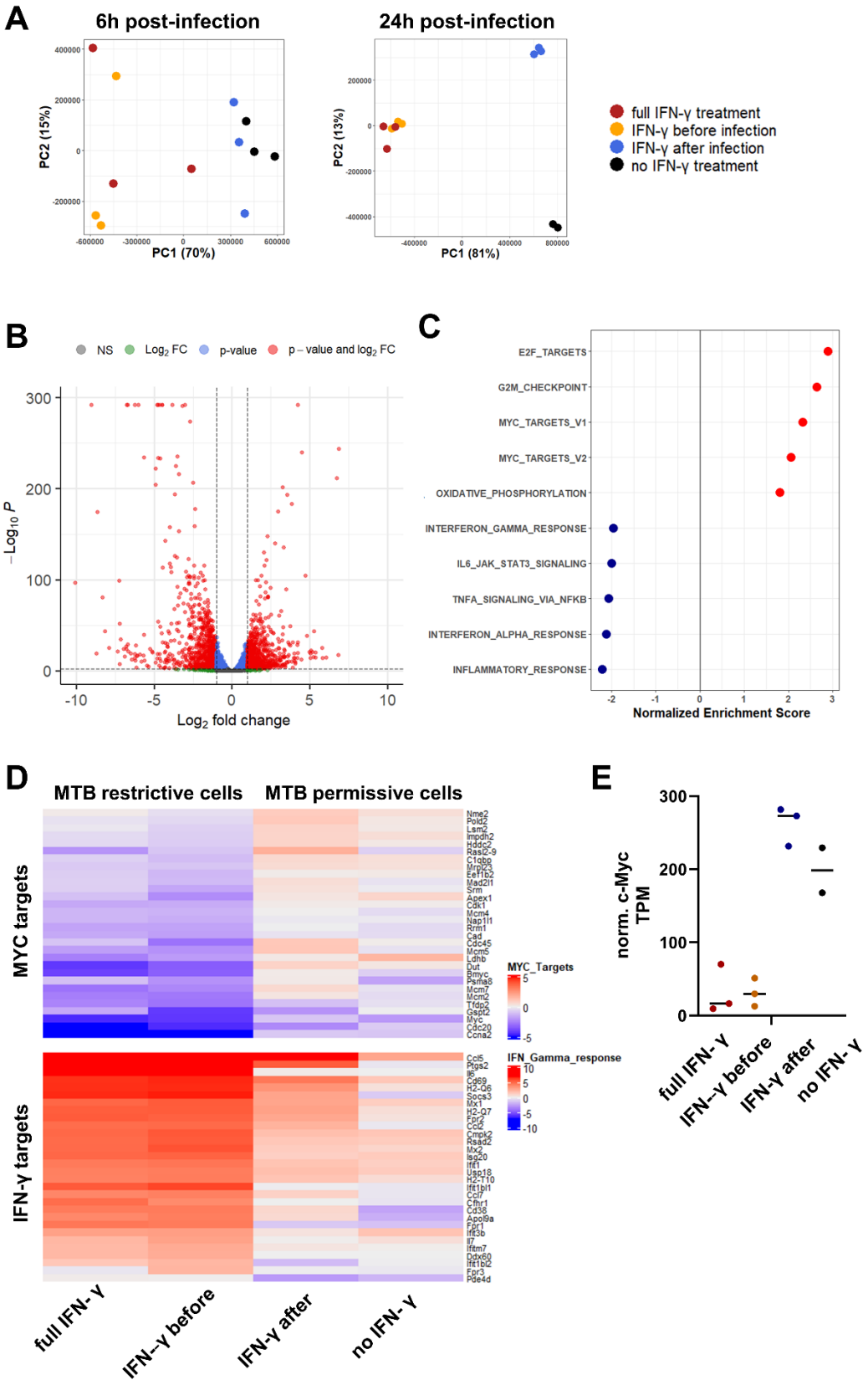
A
6h post-infection
24h post-infection
PC2 (15%)
PC1 (70%)
PC2 (13%)
PC1 (81%)
full IFN-γ treatment
IFN-γ before infection
IFN-γ after infection
no IFN-γ treatment
B
NS
Log2 FC
p-value
p – value and log2 FC
−Log10 P
Log2 fold change
C
E2F_TARGETS
G2M_CHECKPOINT
MYC_TARGETS_V1
MYC_TARGETS_V2
OXIDATIVE_PHOSPHORYLATION
INTERFERON_GAMMA_RESPONSE
IL6_JAK_STAT3_SIGNALING
TNFA_SIGNALING_VIA_NFKB
INTERFERON_ALPHA_RESPONSE
INFLAMMATORY_RESPONSE
Normalized Enrichment Score
D
MTB restrictive cells
MTB permissive cells
MYC targets
IFN-γ targets
MYC_Targets
IFN_Gamma_response
full IFN- γ
IFN–γ before
IFN-γ after
no IFN- γ
E
norm. c-Myc TPM
full IFN- γ
IFN–γ before
IFN-γ after
no IFN- γ

184

Figure 2: Changes in c-Myc associated transcriptional programs mirror MTB permissive versus controlling macrophages *in vitro*

A) Principal Component Analysis (PCA) plot of the first two principal components (PC1 and PC2) of differently activated/infected BMDMs, 6h and 24h after infection with MTB H37Rv (MOI 5). Each point represents an individual sample, with colors indicating the treatment. The percentage of variance explained by each component is shown on the axes. **B)** Volcano plot of differently expressed genes in BMDMs exposed to IFN-γ for 24h after infection versus activated with IFN-γ 24h before infection. Each point represents an individual gene, plotted by $\log_2$ fold-change (x-axis) and $-\log_{10}$ (p-value) (y-axis). Genes with statistically significant differential expression (adjusted $P < 0.05$ and $|\log_2 \text{ fold-change}| > 1$) are highlighted in red. Dashed lines represent *P* value and fold-change thresholds. **C)** Gene Set Enrichment Analysis (GSEA) of BMDMs exposed to IFN-γ for 24h and infected versus firstly infected then exposed to IFN-γ for 24h, showing Normalized Enrichment Score (NES, y-axis) across the Hallmark pathways (x-axis). Only pathways with |NES|>1.5 are shown. GSEA was performed in R with package fgsea (Bioconductor). **D)** Heatmap of Leading Edge Genes among MYC and IFN-γ response pathways, across all conditions 24h after infection. The differential expression is calculated as Mean Log fold Change per condition compared to untreated, uninfected macrophages. BMDMs are labeled restrictive or permissive to MTB growth based on previous CFU results (Figure 1). **E)** Expression of c-Myc mRNA in normalized transcripts per million (TPM) across the four conditions at 24h after infection.

c-Myc inhibition leads to a gain of antimycobacterial function via a distinct transcriptional program

Based on the strong associations reported above, we decided to experimentally perturb c-Myc in macrophages to better understand its role in mycobacterial infections.

To achieve this, we developed a lentiviral system featuring constitutive expression of a truncated nerve growth factor receptor (NGFR) and tetracycline (Tet)-inducible GFP (Supplementary Figure 3). This system was used to transduce bone marrow cells from C57BL/6 mice. After successful transduction, cells were magnetically

sorted and differentiated into BMDMs. When exposed to doxycycline (DOX), a synthetic version derived from tetracycline, these cells expressed GFP, confirming the functionality of our inducible system (Figure 3A).

Next, we replaced GFP with murine c-Myc or Omomyc, a small peptide inhibitor of c-Myc. We confirmed that upon doxycycline stimulation, the transduced cell lines upregulated c-Myc or Omomyc as expected (Figure 3B).

With the system validated, we exposed the transduced BMDMs (Supplementary Figure 4) to doxycycline, infected them with MTB, and performed RNA-seq 24 hours post-infection. The transcriptomic analysis revealed that both c-Myc expression and Omomyc-mediated inhibition had profound effects on the infected cells' transcriptome (Figure 3C). While the significant changes induced by c-Myc overexpression were anticipated - given c-Myc's established role in reprogramming somatic cells into induced pluripotent stem cells[22] - it was particularly striking that Omomyc inhibition also caused extensive transcriptomic alterations.

Subsequent functional enrichment analysis using GSEA indicated that Omomyc-expressing cells exhibited a distinct transcriptional response (Figure 3D). Notably, these cells showed a pronounced upregulation of the tumor necrosis factor (TNF) response, activation of the mTOR1 pathway, and downregulation of IFN-γ responses when compared to wildtype cells. This finding suggests that c-Myc plays a critical role in the regulation of gene expression in mature macrophages in the short term (i.e., 24h), and its downregulation is sufficient to induce changes both in key inflammatory transcriptional responses and the metabolism in macrophages.

To directly assess how c-Myc inhibition impacts MTB growth control, we infected Omomyc- and c-Myc-expressing macrophages with H37Rv. Based on our previous data, we hypothesized that c-Myc inhibition would enhance the macrophages' ability to control MTB growth. Indeed, Omomyc-expressing macrophages demonstrated that c-Myc inhibition led to a significant gain of antimycobacterial activity, comparable to the effect observed with IFN-γ pretreatment (Figure 3E). As an additional control, we tested a commercially available chemical c-Myc inhibitor, 10058-F4, which also led to an increase in antimycobacterial activity, confirming our findings. At the same time, the construct expressing c-Myc had no significant effect on MTB growth.

To understand how these transcriptional changes impacted the macrophages at a cellular level over time, we infected BMDMs with mCherry-expressing H37Rv (Figure 3F) and monitored key functional markers by flow cytometry. As predicted by the transcriptional profile, the Omomyc-expressing macrophages displayed an upregulation of TNF-α on the protein level (Figure 3G). Also, the cells mounted a robust inducible nitric oxide synthase (iNOS) response (Figure 3H). These findings indicated that the macrophages had gained enhanced antimycobacterial function, consistent with the prediction based on transcriptional changes. Importantly, the Omomyc mediated inhibition of c-Myc did not significantly affect macrophage survival compared to control cells as measured with cell viability staining and cell counting, suggesting that the observed changes were specific to the modulation of c-Myc activity rather than a general cytotoxic effect (Supplementary Figure 5).

In conclusion, our data demonstrate that c-Myc is a crucial regulator of macrophage function after MTB infection *in vitro*. Inhibition of c-Myc via Omomyc induces a unique transcriptional profile that, while distinct from classical IFN-γ responses, enhances the antimycobacterial activity of macrophages.

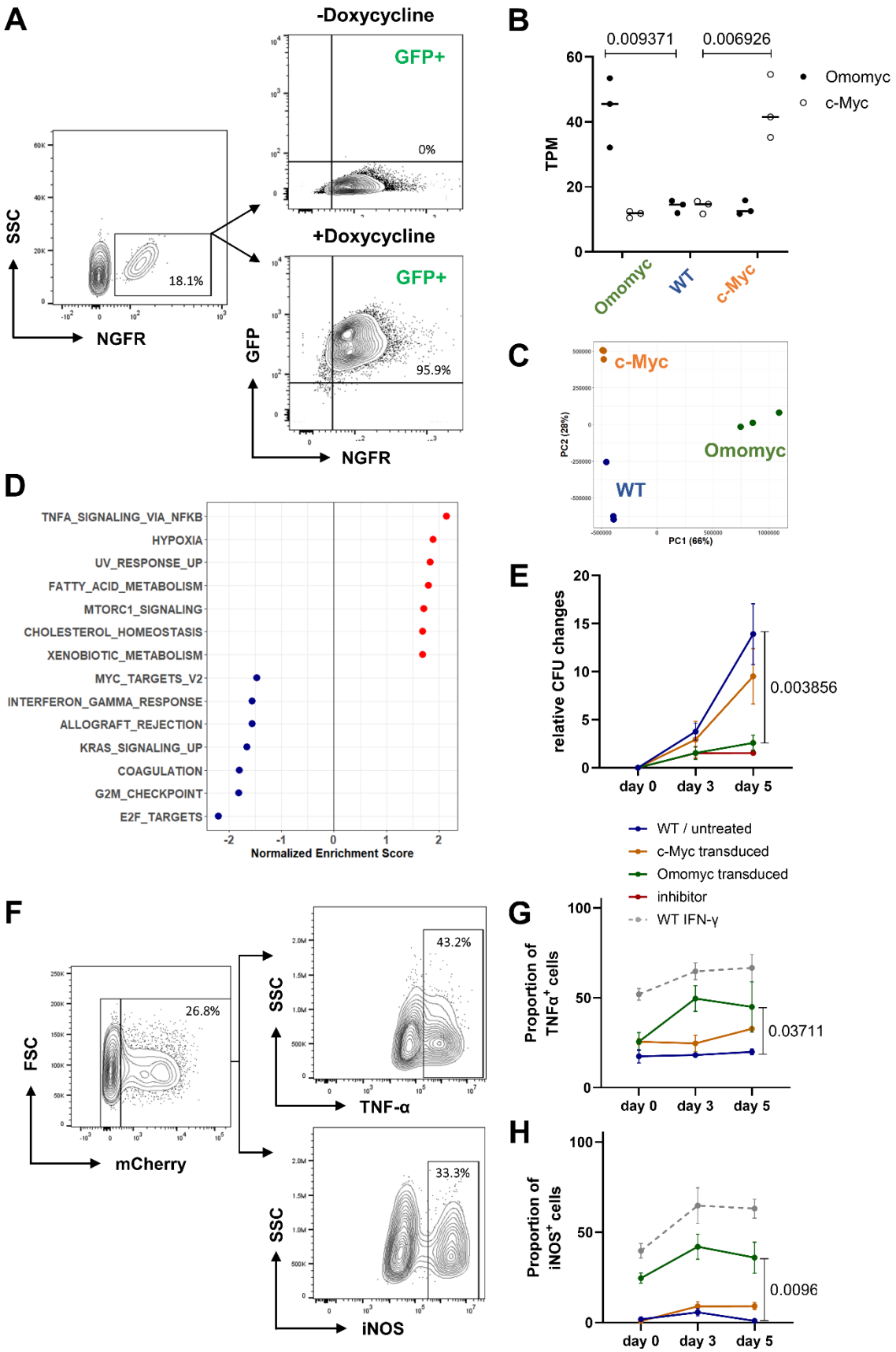
A
-Doxycycline
GFP+
0%
+Doxycycline
GFP+
95.9%
18.1%
SSC
NGFR
GFP
NGFR
B
0.009371
0.006926
TPM
Omomyc
c-Myc
Omomyc
WT
c-Myc
C
c-Myc
Omomyc
WT
PC2 (28%)
PC1 (66%)
D
TNFA_SIGNALING_VIA_NFKB
HYPOXIA
UV_RESPONSE_UP
FATTY_ACID_METABOLISM
MTORC1_SIGNALING
CHOLESTEROL_HOMEOSTASIS
XENOBIOTIC_METABOLISM
MYC_TARGETS_V2
INTERFERON_GAMMA_RESPONSE
ALLOGRAFT_REJECTION
KRAS_SIGNALING_UP
COAGULATION
G2M_CHECKPOINT
E2F_TARGETS
Normalized Enrichment Score
E
relative CFU changes
0.003856
day 0
day 3
day 5
WT / untreated
c-Myc transduced
Omomyc transduced
inhibitor
WT IFN-γ
F
26.8%
FSC
mCherry
43.2%
SSC
TNF-α
33.3%
SSC
iNOS
G
Proportion of TNFα+ cells
0.03711
day 0
day 3
day 5
H
Proportion of iNOS+ cells
0.0096
day 0
day 3
day 5

248

Figure 3: c-Myc inhibition leads to a gain in anti-mycobacterial function and induces a pro-inflammatory phenotype in macrophages *in vitro*

A) Representative flow cytometry plots of BMDMs transduced with lentivirus expressing Tet-on regulated GFP, with or without doxycycline (100ng/mL). Bone marrow cells were sorted 24h after transduction based on the expression of the transduction reporter NGFR. After 6 days, cells were exposed to doxycycline for 24h and assessed using flow cytometry. **B)** RNA expression of c-Myc or the MYC protein inhibitor Omomyc measured as normalized transcripts per million (TPM) in transduced BMDMs (c-Myc and Omomyc under the Tet-on system), after 24h incubation doxycycline (100ng/mL) as measured by RNA-seq. All pairwise statistical comparisons were performed with Student's t-test. **C)** Principal Component Analysis (PCA) plot of the first two principal components (PC1 and PC2) of BMDMs expressing either c-Myc or Omomyc compared to wildtype (WT) after 48h of Tet-on induction with doxycycline and 24h after *in vitro* infection with MTB H37Rv (MOI 5). Each point represents an individual sample, with colors indicating the treatment. The percentage of variance explained by each component is shown on the axes. **D)** Gene Set Enrichment Analysis (GSEA) of BMDMs expressing Omomyc compared to wildtype (WT) after 48h of Tet-on induction with doxycycline and 24h after *in vitro* infection with H37Rv (MOI 5), showing Normalized Enrichment Score (NES, y-axis) across the Hallmark pathways (x-axis). Only pathways with |NES|>1.5 are shown. GSEA was performed in R with package fgsea (Bioconductor). **E)** Relative changes in colony forming units per milliliter (CFU/mL) of intracellular MTB H37Rv in wildtype BMDMs, BMDMs treated with the chemical MYC inhibitor 10058-F4, and in BMDMs expressing c-Myc, Omomyc. Measurements were taken immediately after phagocytosis (day 0) and at 3 and 5 days post-infection. Data represent mean relative changes (range) ± standard deviation from three independent experiments. P values were calculated with Student's t-test between WT and Omomyc-expressing cells. **F)** Flow cytometry plots showing the identification of fully mature BMDMs infected with MTB expressing the fluorescent protein mCherry, based on the fluorescence of mCherry. Further representative plots of the intracellular markers TNF-α and iNOS are shown (condition Omomyc transduced is displayed). **G-H)** Proportion of infected BMDMs expressing TNF-α and iNOS. BMDMs expressing either c-Myc or Omomyc, WT or WT pre-treated with IFN-γ were infected with mCherry-expressing MTB and assessed using flow cytometry at days 0, 3 and 5. Displayed are the mean ± standard deviation of the percentages of infected

cells, defined by gating on mCherry^{+} cells expressing TNF-α and iNOS. *P* values were calculated with Student's t-test between WT and Omomyc-expressing cells.

mTOR mediated metabolic programming explains enhanced antimycobacterial function in c-Myc-inhibition in macrophages

We observed that inhibition of c-Myc via the Omomyc peptide led to significant changes in macrophage functionality, notably an enhancement in antimycobacterial activity. This finding prompted us to investigate the underlying mechanisms, particularly focusing on metabolism. iNOS, which is essential for the production of nitric oxide (NO), a key antimicrobial effector, requires a substantial energy investment, suggesting a need for metabolic reprogramming to support this heightened immune response. Considering the extensive evidence on c-Myc's central role in cellular metabolism, we postulated that c-Myc inhibition might facilitate a metabolic shift that supports enhanced macrophage function. Our transcriptional analysis supported this hypothesis, revealing a marked increase in mTORC1 signaling in c-Myc-inhibited macrophages (Figure 4A). The majority of the upregulated mTORC1 genes were also upregulated in the previous transcriptomic analysis when comparing fully treated macrophages (before and after infection) with untreated, uninfected macrophages (Figure 4B). Therefore, we proposed that the gain of function observed through c-Myc inhibition is driven by metabolic changes mediated by mTORC1.

To investigate this, we conducted *in vitro* infections using mCherry-expressing H37Rv and measured iNOS production with or without mTOR1 inhibition via rapamycin. In line with our hypothesis, rapamycin treatment significantly reduced Omomyc-induced iNOS production (Figure 4C-D), supporting the idea that mTORC1 plays a key role in the increased iNOS expression seen in c-Myc-inhibited BMDMs. We then infected BMDMs with H37Rv. As expected, inhibiting mTOR1 reversed in part the enhanced antimycobacterial function caused by c-Myc inhibition (Figure 4E). This suggests that the improved antimycobacterial activity in c-Myc-inhibited macrophages is partially due to mTOR1 driven changes in metabolism.

Overall, these findings indicate that c-Myc inhibition leads to metabolic reprogramming towards mTOR1, resulting in enhanced macrophage antimicrobial activity.

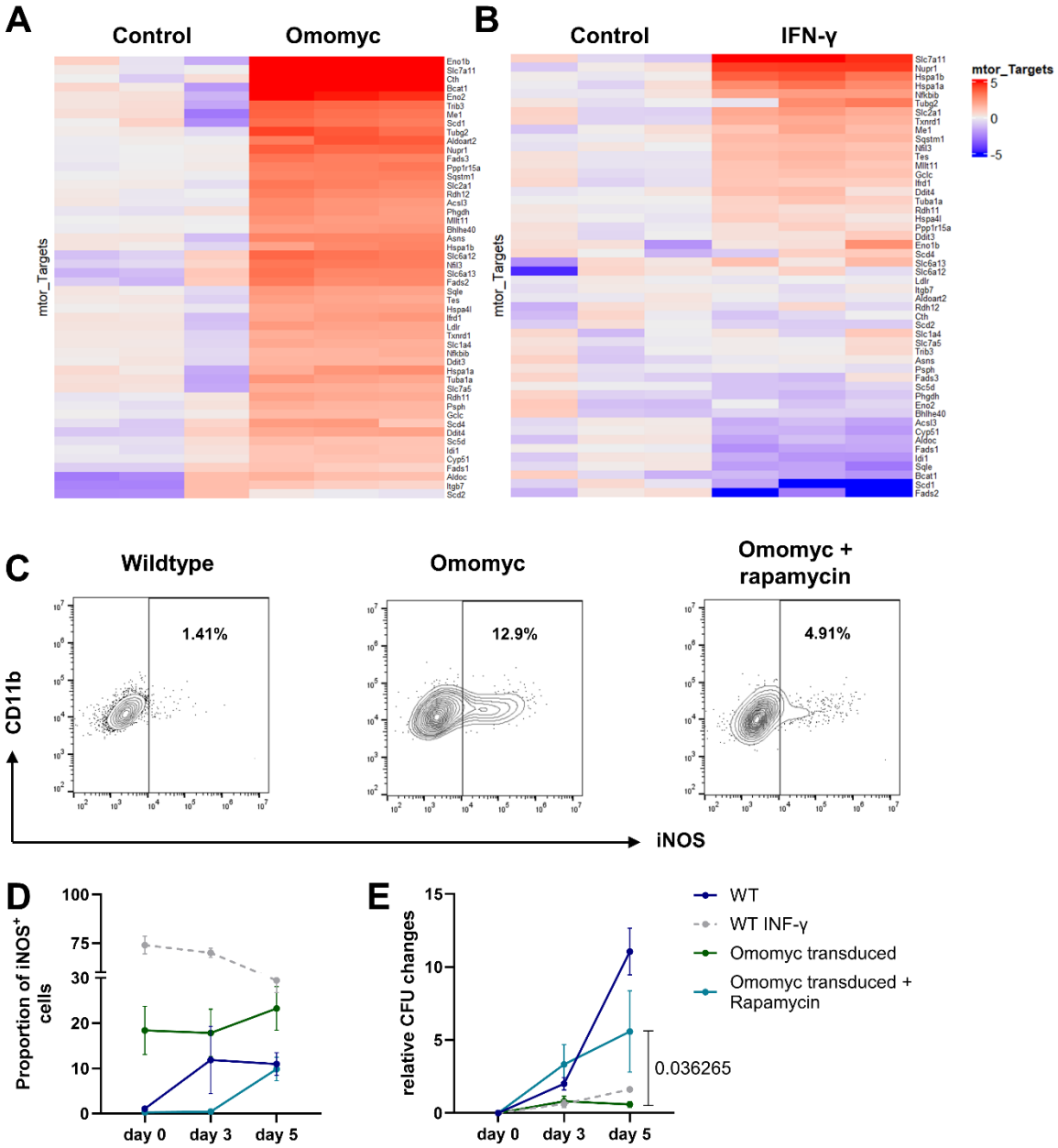

Figure 4: c-Myc inhibition associated gain of antimycobacterial function is partly mediated by a shift towards mTOR1 signaling

A) Heatmap of leading-edge genes identified from gene set enrichment analysis (GSEA) for Hallmark MTORC1 signaling pathway. Rows represent leading-edge genes that contribute most to the enrichment score, while columns represent individual samples from Omomyc-expressing or wildtype BMDMs (control). Genes are expressed as $\log_2$ Fold change from the average of wildtype samples. **B)** Heatmap of the same genes from the previous transcriptomic analysis comparing uninfected, unstimulated BMDMs (control) with infected BMDMs pre-treated with IFN-γ. **C)** Flow cytometry plots displaying iNOS expression in BMDMs infected with mCherry-expressing MTB, at day 3 post-infection. Displayed are wildtype, Omomyc expressing cells and Omomyc-expressing cells treated with rapamycin (10µM). All samples were incubated with the same concentration of DMSO (0.1%). **D)** Proportion of infected BMDMs expressing iNOS in wildtype and Omomyc-expressing BMDMs, compared with Omomyc-expressing BMDMs treated with rapamycin and wildtype BMDMs treated with IFN-γ, at day 0, 3 and 5 post infection. **E)** Relative changes in colony forming units per milliliter (CFU/mL) of intracellular MTB in wildtype BMDMs, Omomyc-expressing BMDMs, Omomyc-expressing BMDMs treated with rapamycin, and wildtype BMDMs treated with IFN-γ. Measurements were taken immediately after phagocytosis (day 0) and at 3 and 5 days post-infection. Data represent mean relative changes (range) ± standard deviation from three independent experiments. *P* values were calculated with Student's t-test between Omomyc-expressing cells and Omomyc-expressing cells treated with rapamycin.

c-Myc is associated with MTB infection in *in vivo* models and in human clinical samples

Given the central role c-Myc played in *in vitro* infections of BMDMs, we aimed to determine whether similar signals could be observed *in vivo*. To this end, we employed the CMTB infection model to investigate an *in vivo* system of asymptomatic MTB infection. As published previously, mice were intradermally infected with 10'000 CFU of MTB H37Rv and allowed to develop a chronic infection over a six-week period[9]. After this time, lymph nodes were harvested, and B and T cells were removed via positive selection using magnetic beads (Figure 5A). The remaining myeloid cells were subjected to single-cell RNA sequencing (scRNA-seq) using the 10X Genomics platform, with subsequent deconvolution of cell populations performed using the Seurat package (Figure 5B-C, Supplementary Figure 6) as published previously[23]. Functional enrichment analysis

focused on monocytes and macrophages, utilizing the AddModuleScore function to calculate the average expression levels of GSEA hallmark c-Myc-related gene programs at the single-cell level[23].

Our analysis demonstrated a significant increase in c-Myc transcriptional programs in monocytes and macrophages during CMTB in mice (Figure 5D). Complementing these findings, a review of RNA-seq data from alveolar macrophages (AM) during MTB infection indicated that AMs with increased bactericidal activity downregulate c-Myc-associated genes[23].

To examine c-Myc expression in lung tissue, we conducted immunohistochemical (IHC) staining with anti-c-Myc antibodies on archived lung tissue sections from prior mouse infection studies (Figure 5E). These studies compared MTB reinfection in mice already with CMTB, and control mice not pre-exposed to MTB from our previously published experiments[9]. Automated image analysis identified c-Myc positive cells and normalized this count to lesion size. At 3 months post-infection, a significant increase in c-Myc-positive cell density was observed within the lesions. Further analysis revealed a positive correlation between lesion size and the number of c-Myc-positive cells. Additionally, a significant interaction was detected between lesion size and experimental group (control vs. CMTB), suggesting that the relationship between lesion size and c-Myc-positive cell count varies by group (Figure 5F). Specifically, as lesion size increases, the control group showed a greater increase in c-Myc-positive cells than the CMTB group (Figure 5G). This indicates that prior MTB exposure in the CMTB model may reduce the accumulation of c-Myc-positive cells or reduce the expression of c-Myc in cells already present as lesions enlarge, potentially contributing to reduced lesion growth. However, while this interpretation aligns with our data, causality cannot be confirmed by these findings alone.

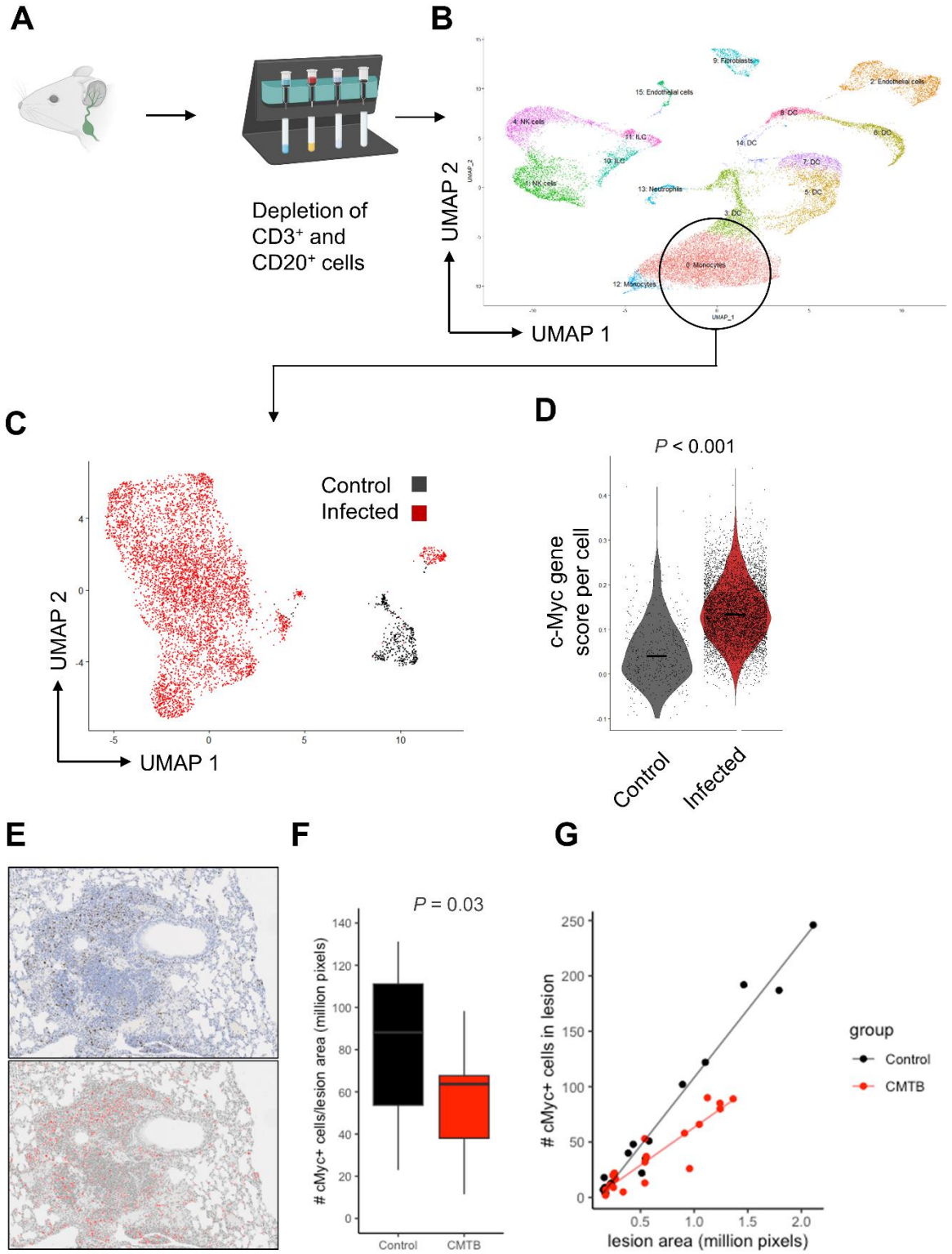
A
B
Depletion of
CD3+ and
CD20+ cells
UMAP 2
UMAP 1
C
Control
Infected
UMAP 2
UMAP 1
D
P < 0.001
c-Myc gene
score per cell
Control
Infected
E
F
P = 0.03
# cMyc+ cells/lesion area (million pixels)
Control
CMTB
G
cMyc+ cells in lesion
lesion area (million pixels)
group
Control
CMTB

350

Figure 5: c-Myc expression is associated with MTB infection in the Contained MTB Infection (CMTB) mouse model of tuberculosis and in the pulmonary infection model

A) Workflow for single-cell RNA sequencing (scRNAseq) of lymph node samples from control and CMTB mice. Adaptive immune cells ($CD3^+$, $CD20^+$ cells) were depleted using magnetic beads. **B)** Compiled scRNAseq data highlighted by major clusters, annotated based on closest Immgen sample match. Circle indicated monocyte/macrophage cluster. **C)** Within the monocyte/macrophage cluster, infected and non-infected cells cluster separately. **D)** Average expression levels of c-Myc genes on single cell level in infected cells and control, subtracted by the aggregated expression of control gene sets. Calculated with AddModuleScore. **E)** Immunohistochemistry (IHC) from pathology slides (previously published[9]) from mice with and without CMTB and stained with an anti c-Myc antibody. Lesion size and number of c-Myc-expressing cells were analyzed using a semiautomated pipeline. **F)** Boxplot showing the density of c-Myc-expressing cells measured as number c-Myc positive cells by lesion area (million pixels) in CMTB mice compared to control. **G)** Correlation between number of c-Myc-expressing cells in a lesion and area of the lesion, in CMTB mice and in control mice.

A key limitation of the mouse model is the absence of granulomas, a hallmark of mycobacterial infections in humans. Granulomas with central necrosis are a defining feature of mycobacterial infections in humans and are structured to contain the pathogen[3]. These granulomas generally have a necrotic core surrounded by an outer layer of immune cells, with the inner granuloma known to be an immune-privileged site. We therefore hypothesized that c-Myc expression may be elevated in the inner granuloma compared to surrounding tissues in humans.

To test this, we analyzed c-Myc expression in human granulomas by comparing its levels relative to the necrotic center. Tissue samples were collected from seven patients diagnosed with active tuberculosis during routine clinical procedures at the University Hospital Zurich (Supplementary Table 1). We used a semi-automated tissue analysis, in which inner and outer granulomas were manually segmented followed by automatic nuclei detection and classification of mean c-Myc staining intensity (Figure 6A). We found a

significantly higher proportion of c-Myc-expressing cells in the inner granuloma than in the outer granuloma (Figure 6B). In addition, c-Myc-positive cells decreased with increasing distance from the core (Figure 6C), and among the positive cells the strength of c-Myc expression also decreased with distance. In summary, c-Myc expression is spatially linked to the immune-privileged environment of the human granuloma.

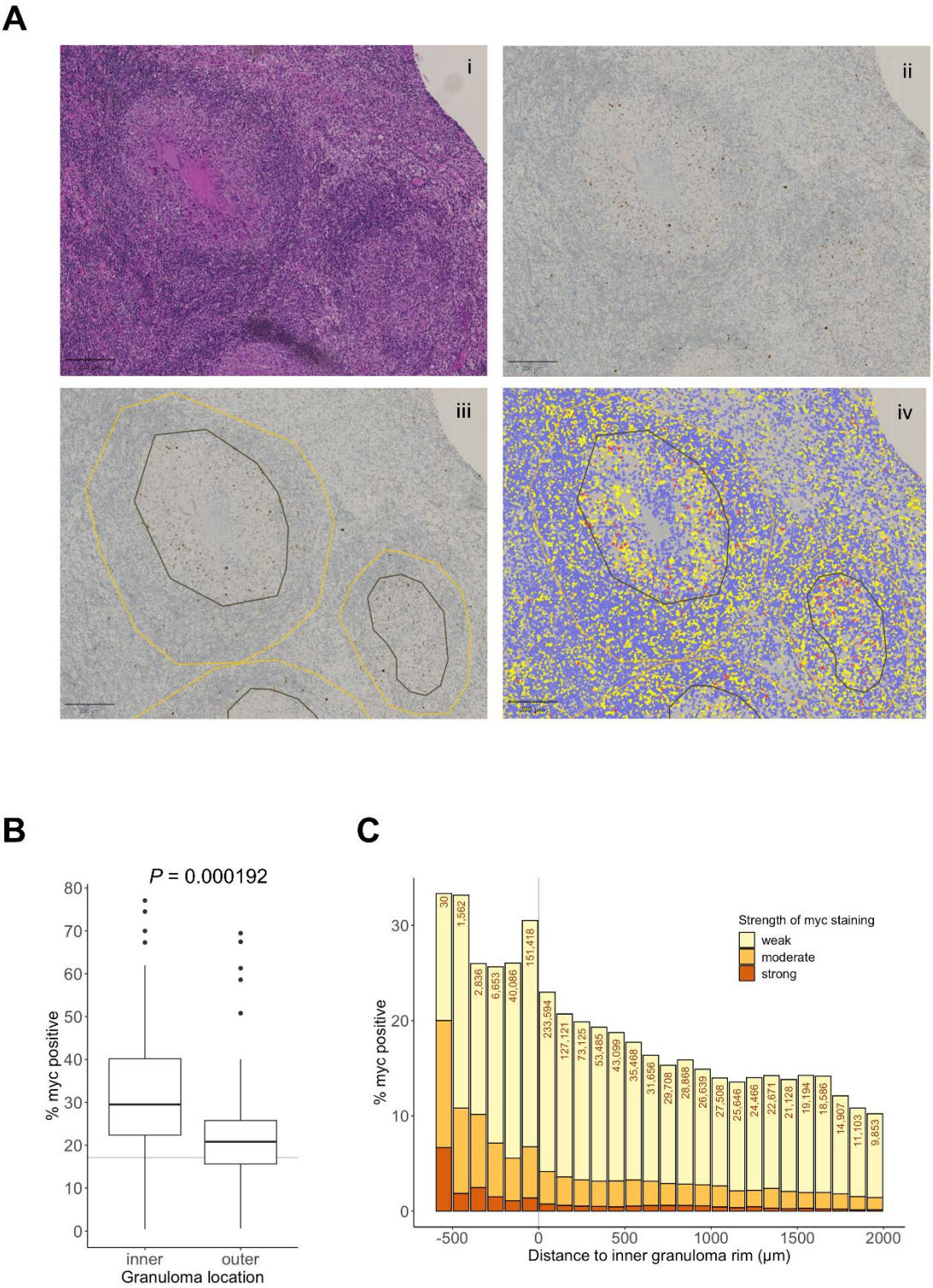

Figure 6: c-Myc expression is associated with the immune privileged niche in the human granuloma during active TB

A) Immunohistochemical stain for myc (i-ii) in inner or outer granuloma. Inner and outer granulomas were manually segmented (iii) followed by automatic nuclei detection and classification of mean myc staining intensity into negative (blue) or positive: weak (yellow), moderate (orange), or strong (red) (iv). **B)** Boxplot showing percent of myc-positive nuclei in granuloma regions; inner granulomas had a higher mean percentage of nuclei positive for myc staining (32.3%) compared to outer granulomas (23.1%), P = 0.000192. The horizontal grey line shows the percentage of positive nuclei outside granulomas (17.1%). **C)** Individual nuclei were grouped by distance to the rim of the nearest inner granuloma into 100 µm bins and the percentages of nuclei with positive staining by intensity were calculated; negative distances indicate the nucleus is within the inner granuloma. The total number of nuclei within each bin is represented at the top.

Discussion

MTB remains a major cause of mortality worldwide. However, over 90% of exposed individuals do not develop active disease, indicating a significant variability in clinical outcomes likely influenced by host immune factors. Based on prior findings and clinical observations, we hypothesized that the activation state of macrophages, particularly the sequence of activation relative to infection, may play a critical role in determining the outcome of MTB exposure. To test this hypothesis, we employed a controlled *in vitro* model to examine the effect of activation timing on macrophage responses to infection. Using an unbiased systems approach, we identified c-Myc as a crucial regulator of anti-mycobacterial activity *in vitro*. Inhibiting c-Myc induced a proinflammatory macrophage phenotype with enhanced anti-mycobacterial properties. Mechanistically, c-Myc inhibition shifted macrophage metabolism towards increased mTOR1 activation, which improved MTB killing.

In line with these findings, inflammation has been linked to suppression of c-Myc associated gene programs[24]. Also, very recent data suggest that overexpression of c-Myc leads to a state of chronic oxidative stress for the macrophage[25]. c-Myc is a crucial regulator in cancer and stem cell biology, known for its role in controlling cell proliferation, growth, and metabolism[26–29]. c-Myc have multiple functions in different cells populations[30–32]. In macrophages, c-Myc has been implicated in the regulation of macrophage polarization[33,34]. While c-Myc has been associated with the outdated M2 macrophage polarization concept as a potential marker of M2 macrophages, its specific functions in mature macrophages have not been thoroughly explored[33,35].

We tackled the experimental challenge of c-Myc inhibition by employing a tetracycline-inducible Omomyc system, which enabled us to differentiate macrophages into their mature form without disruption and subsequently inhibit c-Myc activity post-maturation. Omomyc, a synthetic dominant-negative regulator of c-Myc, competes with c-Myc to form dimers with Max and binds to c-Myc DNA target sequences (E-boxes) preventing the transactivation of the target genes[36]. This approach provides multiple benefits over chemical inhibitors, as it removes the need for solvents and avoid delivery challenges; the inhibitor is instead produced directly inside the target cells.

Our data indicate that c-Myc signaling in mature macrophages significantly contributes to macrophage functionality even in the fully matured cell. Surprisingly, the primary differences between MTB-permissive and

MTB-controlling macrophages occur not in proinflammatory "effector" pathways but in canonical cell cycle pathways. This finding challenges traditional views of c-Myc being key primarily for the development of cells but positions it also a key regulator of mature macrophage responses[24,37–39]. c-Myc inhibition does not immediately kill cells but instead activates a TNF-α[25] and mTORC1-driven transcriptional profile that enhances macrophage function during mycobacterial infection. Our observation that mTORC1 enhances antimycobacterial activity *in vitro* aligns with recent findings from a zebrafish mycobacterial infection model[40].

We found that c-Myc expression and its related transcriptional profiles are strongly associated with MTB infection and active tuberculosis in two different mouse models of MTB infection, as well as in human samples from patients with confirmed active TB. Importantly, the spatial pattern of c-Myc — with up to 30% of cells in the inner granuloma expressing c-Myc during active TB — aligns with the well-established structure of granulomas, where the core is myeloid cell rich and immune-privileged[3]. Since c-Myc is recognized in cancer research as a key regulator of immune privilege, this observation appears intuitive, as granulomas are locally immune-suppressed regions[28]. Additionally, previous studies have identified c-Myc as an essential factor in the formation of multinucleated giant cells, another feature of mycobacterial infections[41]. While we did not specifically examine multinucleated giant cells in this study, and instead focused on c-Myc expression per nucleus rather than per cell, our findings suggest that c-Myc could be a critical mediator of mycobacterial persistence in the host.

The crucial role of c-Myc in survival and inflammatory response makes it a target for specialized intracellular pathogens that must prevent pro-inflammatory activation and promote survival of the infected cells in order to proliferate. Indeed, upregulation of c-Myc have been reported in cells infected with *Chlamydia trachomatis* [42–44], *Salmonella typhimurium*[45] and the protozoan pathogen *Leishmania donovani*[46], demonstrating that this mechanism evolved independently in different intracellular pathogens. Furthermore, repression of c-Myc signaling alone has been proved to reduce bacterial growth in *Chlamydia* [43,44,46]. These results suggest that c-Myc may play a significant role in intracellular infections in general.

Our data indicate that c-Myc inhibition leads to significant upregulation of mTORC1. Reduced activity of mTORC1 subsequently results in decreased iNOS production and partially reverses the enhanced

antimycobacterial activity observed with c-Myc inhibition, suggesting that mTORC1 activity is critical for this gain of function. Furthermore, mTORC1 is also upregulated following IFN-γ stimulation, as confirmed by our experiments and supported by previous findings showing that BMDMs increase mTORC1 activation upon IFN-γ exposure[47]. The metabolic profile resembles the trained immunity phenotype, which also leads to a gain of antimicrobial functions in myeloid cells[48]. Interestingly, however, canonical IFN-γ responsive genes are downregulated in c-Myc inhibited BMDMs, indicating a divergence from typical IFN-γ driven responses. These findings suggest that metabolic adaptations, such as mTORC1-mediated shifts, may be as influential in the control of MTB infection *in vitro* as the traditional IFN-γ pathways, highlighting the importance of metabolic reprogramming in host antimicrobial defense mechanisms.

The primary limitation of this study is the absence of *in vivo* data to demonstrate the effects of c-Myc perturbation on MTB infection, such as, for example, in a mouse model. Although future studies will address this, we have observed strong *in vivo* associations, including the immune privileged core of human granulomas[3,8,17], where MTB is located.

In conclusion, our data show that c-Myc signaling plays a major role in influencing anti-mycobacterial responses in macrophages *in vitro*. The strong *in vivo* association in both small animal models and in human tissues from patients suffering from active TB support further investigation into the interactions between c-Myc and mycobacterial infections.

Materials

Key Resource Table

REAGENT OR RESOURCE	SOURCE	IDENTIFIER
Cells		
Bone marrow-derived macrophages	*Produced by authors from C57BL/6 mice*	n/a
HEK 293T	ATCC	CRL-1573
Mouse Strains		
C57BL/6J wildtype	Charles River Laboratories	C57BL/6J
Bacterial Strains		
Escherichia coli Stbl2™ Competent Cells	Invitrogen	10268019
Mycobacterium tuberculosis H37Rv	*Provided by Prof. Alan Aderem*	n/a
Mycobacterium tuberculosis H37Rv – live-dead reporter	*Provided by Prof. Sarah Fortune*	n/a
Mycobacterium tuberculosis H37Rv - mCherry	*Provided by Prof. Alan Aderem*	n/a

Antibodies and Fluorescent Dyes

Anti-human CD271 (NGFR)-APC	Biolegend	345108
Anti-human CD271 (NGFR)-PE	Biolegend	345106
Anti-mouse CD16/CD32-TruStain FcX	Biolegend	101320
Anti-mouse CD206-AF700	Biolegend	141734
Anti-mouse CD80-BV421	Biolegend	104725
Anti-mouse CD86-APC	Biolegend	105114
Anti-mouse F4/80-PerCP-Cy5.5	Biolegend	123127
Anti-mouse iNOS-APC	Thermo Fisher Scientific	17-5920-82
Anti-mouse MHC-II (I-A/I-E)-PE/Cy7	Biolegend	107630
Anti-mouse TNFa-PE-Dazzle 594	Biolegend	506346
Anti-mouse/human CD11b-BV605	Biolegend	101237
Zombie NIR™ Fixable Viability Kit	Biolegend	423105

Chemicals for Bacterial Culture

BBL™ Middlebrook OADC Enrichment	BD Life Science	212351
Difco™ Middlebrook 7H10 Agar	BD Life Science	262710
Difco™ Middlebrook 7H9 Broth	BD Life Science	271310
Glycerol 87%	AppliChem	A3739
Hygromycin B Gold	InvivoGen	HGG-40-01
Kanamycin	Calbiochem	420311

Polysorbate 80	Hänseler	267380-02

Chemicals, Peptides, and Recombinant Proteins for Cell Culture

c-Myc inhibitor 10058-F4	Merck-Sigma	475956-10MG
DMEM	Sigma-Aldrich	D5796
EDTA	ITW Reagents	A4892
FBS	Thermo Fisher Scientific	26140
Lenti-X GoStix Plus	Takara	631280
L-glutamine	Thermo Fisher Scientific	25030081
Mouse IFN-γ Recombinant Protein	Biolegend	575306
Mouse M-CSF Recombinant Protein	Biolegend	576406
Mouse SCF Recombinant Protein	Biolegend	579704
Mouse TPO Recombinant Protein	Biolegend	593304
Opti-MEM™	Thermo Fisher Scientific	11058021
PBS	Sigma-Aldrich	D8537
Penicillin-Streptomycin	Thermo Fisher Scientific	15140148
Polyethylenimine	Thermo Fisher Scientific	BMS1003-A
Protamine sulfate	Sigma-Aldrich	P4380
PVA	Sigma-Aldrich	P8136

RPMI-1640	Merck-Sigma	R8758
Sodium azide	Sigma-Aldrich	S2002
StemSpan™ SFEM	STEMCELL Technologies	9600

Commercial Kits

Cyto-Fast™ Fix/Perm Buffer Set	Biolegend	426803
Direct Lineage Cell Depletion Kit (mouse)	Miltenyi	130-110-470
QIAshredder	Qiagen	79656
RNase-Free DNase Set	Qiagen	79254
RNeasy Mini Kit	Qiagen	4106

DNA Sequences and Plasmids

c-Myc	ENSEMBL	ENSMUSG00000022346
Omomyc	Soucek et al., 1998	n/a
P8.9Δ	AddGene	132929
pMD2.G	AddGene	187440
pTRE3G-GSX2	AddGene	96964
pVPX	Pertel et al., 2011	n/a

Software and Algorithms

FlowJo™ Software (10.0.8)	FlowJo LLC, Ashland, OR: Becton, Dickinson and Company; 2023
GraphPad Prism (10.3.1)	GraphPad Software, Inc.

R Studio (2024.09.0)	RStudio Team, RStudio: Integrated Development for R. RStudio, PBC, Boston, MA http://www.rstudio.com/

Experimental models

MTB strains

MTB strain H37Rv and H37Rv mCherry Fluorescent MTB strains were kindly provided by Prof. Alan Aderem. MTB H37Rv live-dead reporter strain was provided by Prof. Sarah Fortune. All strains were cultured in Difco™ Middlebrook 7H9 supplemented with 10%(v/v) BBL™ Middlebrook OADC and polysorbate 80 in roller bottles or Difco™ Middlebrook 7H10 Agar supplemented with 10%(v/v) BBL™ Middlebrook OADC and 0.5% (v/v) Glycerol 87%. Kanamycin (30 µg/mL) and hygromycin B (50 µg/mL) were added to the mCherry strain and the live-dead strain respectively. Bacteria were quantified by spectrophotometry (OD 600nm).

Mouse strains

C57BL/6J female mice were bought from Charles River Laboratories and were used as donor for bone marrow macrophages production. All procedures were approved by the cantonal animal experimentation authorities and conformed to international guidelines for laboratory animal experimentation (Canton of Zurich, licenses ZH138/19 and ZH041/21). All mice were maintained on a 12h light-dark cycle under clean, conventional (i.e. specific pathogen-free) conditions and with free access to water and food.

Methods

Cell culture and cell isolation from bone marrow

HEK 293T cells were cultured in Dulbecco's Modified Eagle Medium (DMEM) supplemented with 10% fetal bovine serum (FBS), 1% L-glutamine (2 mM), and 1% Penicillin-Streptomycin (100 U/mL penicillin and 100 µg/mL streptomycin; P/S). Bone marrow cells were harvested as described by Amend et al.[50]. To induce differentiation into bone marrow-derived macrophages (BMDMs), bone marrow cells were cultured in Roswell Park Memorial Institute (RPMI)-1640 medium supplemented with 10% FBS, 1% L-glutamine, 1% P/S, and 50

ng/mL macrophage colony-stimulating factor (M-CSF) at a density of 2×10^6 cells/mL. The medium was refreshed on day 3. On day 6, non-adherent suspension cells were discarded, and adherent cells were detached (with cold PBS + EDTA (5mM) by pipetting) for downstream experiments. To isolate hematopoietic stem cells (HSCs) and immune progenitors from the bone marrow, negative magnetic selection was performed using the Direct Lineage Cell Depletion Kit following the manufacturer's protocol. Bone marrow hematopoietic progenitors were grown in 6-well plates with HSC medium (StemSpan SFEM medium supplemented with 1 mg/ml polyvinyl alcohol (PVA), 50 ng/ml thrombopoietin (TPO), and 100 ng/ml stem cell factor (SCF)), adapted from Wilkinson et al[51].

Cloning of the Tet-on system into lentiviral vectors

rtTA V16, an improved version of the reverse tetracycline transactivator used in Tet-on systems was developed by Das et al.[52]. TRE3G inducible promoter was obtained from plasmid pTRE3G-GSX2. Omomyc peptide sequence was obtained from Soucek et al.[53], and inserted in the construct. The coding sequence of the murine version of c-Myc was obtained from the ENSEMBL database.

Production of lentiviral particles

Lentiviruses were generated by transfecting HEK 293T cells with lentiviral vectors in Opti-MEM using polyethylenimine (PEI) as the transfection reagent. The transfection mix included p8.9Δ (containing the coding sequences for gag/pol, rev, and tat under the control of the immediate/early promoter enhancer of cytomegalovirus), pMD2.G (encoding vesicular stomatitis virus glycoprotein), and a VPX-expressing plasmid (as described by Pertel et al.[55]) in a 1:3 DNA-to-PEI ratio. The medium was replaced 16h post-transfection with RPMI supplemented with 5% FBS. Supernatants containing lentiviral particles were collected and filtered 48h after transfection. Lentiviral production was confirmed using the Lenti-X GoStix Plus assay. Viral particles were subsequently concentrated by centrifugation at 20'000g for 2h, resuspended in PBS, and stored at −80°C until further use.

Transduction of mouse HSCs and myeloid progenitors

HSCs and immune progenitors were isolated from mice as described above and cultured overnight in HSC medium (described above). For transduction, the medium was prepared by supplementing the HSC medium with 10 µg/mL protamine and the appropriate lentiviruses at a multiplicity of infection (MOI) of 10. Cells were resuspended in the transduction medium at a density of 1×10^6 cells/mL. After 12 hours of incubation, the cells were pelleted by centrifugation, washed with PBS, and resuspended in RPMI medium supplemented with 10% FBS, 1% L-glutamine, and 50 ng/mL M-CSF to promote differentiation into macrophages/BMDMs.

Macrophage infection assays

BMDMs were seeded in 96 well plates, $7x10^5$ cells per well, in RPMI supplemented with 10% FBS and 1% L-glutamine and 50ng/mL M-CSF. After 24h of rest the cells were treated with IFN-γ 25ng/mL according to condition. On the day of infection, bacteria in log-phase (OD 0.1-0.5) were pelleted by centrifugation and resuspended in RPMI and used to infect BMDMs. BMDMs were infected at a MOI of 5 bacilli per macrophage for 1h at 37°C and washed twice with PBS to remove extracellular bacteria. The cells were provided fresh media (RPMI with 50 ng/mL M-CSF) and with or without IFN-γ according to conditions. For assays without IFN-γ but involving Tet-on constructs (c-Myc- and Omomyc-expressing BMDMs), the media was supplemented with doxycycline (100 ng/mL) 24h prior to infection and maintained throughout the experiment. At day 0 (after infection), 3 and 5 the macrophages were detached from the wells with cold PBS + EDTA (5mM) by pipetting gently. Half of the suspension with the cells were either used for flow cytometry staining or lysed with 0.05% SDS in water, and the lysate was plated on 7H10 agar plates in serial dilutions. After 3 weeks of incubation at 37°C colonies were counted to measure the anti-bacterial activity of macrophages.

Flow cytometry staining

Staining was performed in FACS buffer (PBS + 2mM EDTA + 2% FBS + 0.1% sodium azide) containing CD16/CD32 blocker (FcX), Zombie NIR dye and the fluorescent antibodies (= master mix). Suspension cells were pelleted by centrifugation at 300g for 5min and washed once prior to staining. BMDMs were detached by removing the media, washing with PBS, and incubating the cells for 5-10min in cold PBS + EDTA (5 mM),

553 followed by gentle pipetting to detach the cells. Cells were incubated in the master mix for 20min in the fridge.
554 Cells were washed and fixed in 2–4% paraformaldehyde (PFA) at room temperature for 20min, with particular
555 emphasis on MTB-infected cells. For intracellular staining, the Cyto-Fast™ Fix/Perm Buffer Set was used
556 according to the manufacturer's instructions before fixation.

557 **Mouse infection experiments**

558 All mouse experiments regarding the CMTB model have been previously reported in Nemeth *et al.*[9]. For
559 completeness, we briefly describe the establishment of CMTB using intradermal ear injection and aerosol
560 infection. Intradermal infections involved administering 10'000 CFU of logarithmic-phase MTB H37Rv in 10µL
561 PBS using a 10µL Hamilton syringe into mice anesthetized with ketamine, following a modified protocol.
562 Aerosol infections were performed using a diluted frozen stock of kanamycin-resistant MTB H37Rv in an
563 aerosol infection chamber (Glas-Col). Bacterial load was assessed by plating serial dilutions of homogenized
564 tissue on kanamycin-containing and antibiotic-free plates to differentiate between the sources of infection.

565 **RNA sequencing**

566 For bulk RNA-seq experiments, 1×10^6 BMDMs per well were seeded in 12-well plates RNA was extracted
567 with the RNeasy Kit (QIAGEN), in combination with QIAshredder columns (QIAGEN) and DNase Set
568 according to the manufacturer's protocol. Library construction, sequencing and data analysis was conducted
569 by the Functional Genomic Center of Zurich. Libraries were assembled with TruSeq® Stranded mRNA Library
570 Prep and Sequencing was performed with Ilumina NovaSeq 6000. Transcripts were quantified with kallisto
571 software and data analysis was performed in R with packages DeSeq2.

572 **Single cell RNA sequencing**

573 Lymph nodes were obtained from mice with and without CMTB (n = 5 per condition). Following isolation,
574 samples underwent methanol fixation according to protocol "CG000136 Rev. D" from 10X Genomics. Briefly,
575 samples were filtered using 70 µm filters, and red blood cells were lysed with ACK lysis buffer. Post-lysis, cells
576 were resuspended in 1mL of ice-cold PBS with a wide-bore pipette, then transferred to a 1.5mL low-bind
577 Eppendorf tube. After centrifugation at 700g for 5min at 4°C, the supernatant was carefully discarded, and the

cell pellet was washed twice with PBS, counted, and resuspended in 200µL of ice-cold PBS per 1×10^6 cells. To achieve an 80% final methanol concentration, 800µL of ice-cold methanol was gradually added to the suspension. The samples were incubated at -20°C for 30min and stored at -80°C for up to six weeks prior to rehydration.

For rehydration, samples were thawed at 4°C, centrifuged at 1’000g for 10min at 4°C, and resuspended in 50µL of a wash-resuspension buffer (0.04% BSA, 1mM DTT, 0.2U/µL Protector RNAase Inhibitor in 3X SSC buffer) to achieve a final concentration of approximately 1’000 cells/µL, accounting for an estimated 75% cell loss.

Single cell RNA sequencing analysis

Libraries were constructed using the Next GEM Single Cell 3’ Reagent Kits v3.1 (Dual Index) from 10X Genomics, following the manufacturer’s protocol. Sequencing data were aligned to the mouse genome (mm10), and unique molecular identifier (UMI) counts were calculated using the Cell Ranger pipeline. Data processing, integration, and downstream analysis were conducted in Seurat v3, with quality control filtering to exclude droplets containing fewer than 200 detected genes, more than 4’000 detected genes (to discriminate against doublets), or more than 5% mitochondrial gene expression. Genes detected in fewer than three cells across all samples were excluded. Cell-type annotation leveraged the Immgen database as a reference, implemented with the "SingleR" package. Additionally, pseudotime trajectory analysis was performed using "SeuratWrappers" and "Monocle3." Data visualization was facilitated using the "Seurat," "tidyverse," "cowplot," and "viridis" R packages.

Mouse histology

Immunohistochemistry for c-Myc was performed at the University of Washington Histology and Imaging Core and scanned images were exported to tiffs and then uploaded into ImageJ. Areas of consolidation were identified on images converted to 8-bit grayscale and thresholded using the “Triangle” method. After signal noise reduction with a median filter, sequential minimum and maximum filters were used to identify areas of true consolidation. c-Myc$^+$ cells were identified by color-thresholding to identify brown (DAB$^+$) cells against the

background of blue nuclei and these were automatically counted within each consolidated lesion by using the analyze particles command. The c-Myc^{+} cell density within each consolidated lesion was calculated as the number of c-Myc^{+} cells per million pixels. Statistical analysis was with a two-sided t-test.

Human histology

Patients with confirmed tuberculosis (Culture and/or PCR positive) who had a histological specimen available and had agreed in written to the further use of their routinely obtained specimens for science were included after Ethical Clearance from the Ethical committee from Zurich was given. Specimens were stained with H&E and anti-c-Myc antibody using routine clinical protocols. The tissues were fixed, photographed and transformed into NDPI files, which were loaded into QuPath and granulomas (both caseating and non-caseating) were identified on hematoxylin and eosin stained slides[56]. Manual segmentation with QuPath's polygon tool was used to create annotations for inner and outer; the inner region was subtracted from the outer region to create non-overlapping annotations. To calculate the percentage of non-epithelial cells outside granulomas that express myc, an automatic threshold was applied to the myc stained slides based on the average RGB intensity to identify all tissue. Areas of epithelium and the previously defined granuloma regions were excluded from the background tissue region. Additional annotations were created to exclude areas of artifact (e.g., folded tissue). Positive cell detection with the following parameters ('{"detectionImageBrightfield":"Opticaldensitysum","requestedPixelSizeMicrons":0.5,"backgroundRadiusMicrons":15.0,"backgroundByReconstruction":true,"medianRadiusMicrons":0.0,"sigmaMicrons":1.5,"minAreaMicrons":10.0,"maxAreaMicrons":400.0,"threshold":0.12,"maxBackground":2.0,"watershedPostProcess":true,"excludeDAB":false,"cellExpansionMicrons":2.0,"includeNuclei":true,"smoothBoundaries":true,"makeMeasurements":true,"thresholdCompartment":"Nucleus: DAB OD mean","thresholdPositive1":0.18,"thresholdPositive2":0.3,"thresholdPositive3":0.5,"singleThreshold":false}') was used to automatically identify nuclei and classify them into negative, positive (weak), positive (moderate), or positive (strong) myc staining. Separate quantifications at the annotation (i.e. granuloma region) level and the detection (i.e. nuclei) level were exported and analyzed using R.

Lead contact and material availability

Requests for further information and resources should be directed to and will be fulfilled by the lead contact, Johannes Nemeth (johannes.nemeth@usz.ch).

Author contributions

J.N. conceived the study and co-designed the experiments with E.S. and C.D.. E.S., C.D., R.W., D.M., and D.R. performed the experiments. K.K., J.H.R., L.B., and G.S.O. analyzed (single-cell) RNA sequencing and histology data and provided critical insights. S.B. advised on plasmid design and lentivirus production. M.G., P.S., A.H.D., and R.F.S. provided critical advice on project progression and data analysis. J.N., C.D., and E.S. wrote the manuscript.

Acknowledgements

The work was supported by the Swiss National Science Foundation (SNSF) grant 310030_200407 to J.N.. Work in the laboratory of P.S. is supported by SNSF grant 310030_197699/1, the Federal Office of Public Health (3632001500), and University of Zurich. The authors used large language models (ChatGPT, specifically GPT-3.5 and GPT-4, developed by OpenAI) to enhance the clarity and readability of the manuscript. After using this tool, the authors reviewed and edited the content as necessary and take full responsibility for the content of the published article.

Declaration of interest

The authors have declared that no competing interests exist. J. N. received honoraria for presentations and advisory boards from Oxford Immunotec, Gilead and ViiV.

References

1. Global Tuberculosis Report 2023.

2. Flynn, J.L., and Chan, J. (2022). Immune cell interactions in tuberculosis. Cell *185*, 4682–4702. https://doi.org/10.1016/j.cell.2022.10.025.

3. Cohen, S.B., Gern, B.H., and Urdahl, K.B. (2022). The Tuberculous Granuloma and Preexisting Immunity. Annu Rev Immunol *40*, 589–614. https://doi.org/10.1146/annurev-immunol-093019-125148.

4. Lin, P.L., Ford, C.B., Coleman, M.T., Myers, A.J., Gawande, R., Ioerger, T., Sacchettini, J., Fortune, S.M., and Flynn, J.L. (2013). Sterilization of granulomas is common in active and latent tuberculosis despite within-host variability in bacterial killing. *20*, 75–79. https://doi.org/10.1038/nm.3412.

5. Cadena, A.M., Fortune, S.M., and Flynn, J.L. (2017). Heterogeneity in tuberculosis. Nature Publishing Group *27*, 1–12. https://doi.org/10.1038/nri.2017.69.

6. Lenaerts, A., Barry, C.E., and Dartois, V. (2015). Heterogeneity in tuberculosis pathology, microenvironments and therapeutic responses. Immunological reviews *264*, 288–307. https://doi.org/10.1111/imr.12252.

7. Plumlee, C.R., Duffy, F.J., Gern, B.H., Delahaye, J.L., Cohen, S.B., Stoltzfus, C.R., Rustad, T.R., Hansen, S.G., Axthelm, M.K., Picker, L.J., et al. (2021). Ultra-low Dose Aerosol Infection of Mice with Mycobacterium tuberculosis More Closely Models Human Tuberculosis. Cell Host Microbe *29*, 68-82.e5. https://doi.org/10.1016/j.chom.2020.10.003.

8. Gideon, H.P., Hughes, T.K., Tzouanas, C.N., Wadsworth, M.H., Tu, A.A., Gierahn, T.M., Peters, J.M., Hopkins, F.F., Wei, J.-R., Kummerlowe, C., et al. (2022). Multimodal profiling of lung granulomas in macaques reveals cellular correlates of tuberculosis control. Immunity. https://doi.org/10.1016/j.immuni.2022.04.004.

9. Nemeth, J., Olson, G.S., Rothchild, A.C., Jahn, A.N., Mai, D., Duffy, F.J., Delahaye, J.L., Srivatsan, S., Plumlee, C.R., Urdahl, K.B., et al. (2020). Contained Mycobacterium tuberculosis infection induces concomitant and heterologous protection. PLoS pathogens *16*, e1008655-25. https://doi.org/10.1371/journal.ppat.1008655.

10. Cadena, A.M., Hopkins, F.F., Maiello, P., Carey, A.F., Wong, E.A., Martin, C.J., Gideon, H.P., DiFazio, R.M., Andersen, P., Lin, P.L., et al. (2018). Concurrent infection with Mycobacterium tuberculosis confers robust protection against secondary infection in macaques. PLoS pathogens *14*, e1007305-17. https://doi.org/10.1371/journal.ppat.1007305.

11. Andrews, J.R., Noubary, F., Walensky, R.P., Cerda, R., Losina, E., and Horsburgh, C.R. (2012). Risk of Progression to Active Tuberculosis Following Reinfection With Mycobacterium tuberculosis. Clinical Infectious Diseases *54*, 784–791. https://doi.org/10.1093/cid/cir951.

12. Ivashkiv, L.B. (2018). IFNγ: signalling, epigenetics and roles in immunity, metabolism, disease and cancer immunotherapy. Nature reviews. Immunology *18*, 1–14. https://doi.org/10.1038/s41577-018-0029-z.

13. Flynn, J.L. (1993). An essential role for interferon gamma in resistance to Mycobacterium tuberculosis infection. Journal of Experimental Medicine *178*, 2249–2254. https://doi.org/10.1084/jem.178.6.2249.

14. Hu, X., and Ivashkiv, L.B. (2009). Cross-regulation of Signaling Pathways by Interferon-γ: Implications for Immune Responses and Autoimmune Diseases. Immunity *31*, 539–550. https://doi.org/10.1016/j.immuni.2009.09.002.

15. Huaman, M.A., Jr, G.S.D., and Fichtenbaum, C.J. (2016). Elevated Circulating Concentrations of Interferon-Gamma in Latent Tuberculosis Infection. Pathogens and Immunity *1*, 291–13. https://doi.org/10.20411/pai.v1i2.149.

16. Aggarwal, A.N., Agarwal, R., Dhooria, S., Prasad, K.T., Sehgal, I.S., and Muthu, V. (2020). Unstimulated Pleural Fluid Interferon Gamma for Diagnosis of Tuberculous Pleural Effusion: a Systematic Review and Meta-analysis. J. Clin. Microbiol. *59*, 10.1128/jcm.02112-20. https://doi.org/10.1128/jcm.02112-20.

17. McCaffrey, E.F., Donato, M., Keren, L., Chen, Z., Delmastro, A., Fitzpatrick, M.B., Gupta, S., Greenwald, N.F., Baranski, A., Graf, W., et al. (2022). The immunoregulatory landscape of human tuberculosis granulomas. Nat. Immunol. *23*, 318–329. https://doi.org/10.1038/s41590-021-01121-x.

18. Ramakrishnan, L. (2012). Revisiting the role of the granuloma in tuberculosis. Nat Rev Immunol *12*, 352–366. https://doi.org/10.1038/nri3211.

19. Martin, C.J., Booty, M.G., Rosebrock, T.R., Nunes-Alves, C., Desjardins, D.M., Keren, I., Fortune, S.M., Remold, H.G., and Behar, S.M. (2012). Efferocytosis Is an Innate Antibacterial Mechanism. Cell Host Microbe *12*, 289–300. https://doi.org/10.1016/j.chom.2012.06.010.

20. Bryson, B.D., Rosebrock, T.R., Tafesse, F.G., Itoh, C.Y., Nibasumba, A., Babunovic, G.H., Corleis, B., Martin, C., Keegan, C., Andrade, P., et al. (2019). Heterogeneous GM-CSF signaling in macrophages is associated with control of Mycobacterium tuberculosis. Nat. Commun. *10*, 2329. https://doi.org/10.1038/s41467-019-10065-8.

21. Irvine, E.B., Nikolov, A., Khan, M.Z., Peters, J.M., Lu, R., Sixsmith, J., Wallace, A., Woudenbergh, E. van, Shin, S., Karpinski, W., et al. (2024). Fc-engineered antibodies promote neutrophil-dependent control of Mycobacterium tuberculosis. Nat. Microbiol. *9*, 2369–2382. https://doi.org/10.1038/s41564-024-01777-9.

22. Okita, K., Ichisaka, T., and Yamanaka, S. (2007). Generation of germline-competent induced pluripotent stem cells. Nature *448*, 313–317. https://doi.org/10.1038/nature05934.

23. Mai, D., Jahn, A., Murray, T., Morikubo, M., Lim, P.N., Cervantes, M.M., Pham, L.K., Nemeth, J., Urdahl, K., Diercks, A.H., et al. (2024). Exposure to Mycobacterium remodels alveolar macrophages and the early

innate response to Mycobacterium tuberculosis infection. PLOS Pathog. *20*, e1011871. https://doi.org/10.1371/journal.ppat.1011871.

24. Liu, L., Lu, Y., Martinez, J., Bi, Y., Lian, G., Wang, T., Milasta, S., Wang, J., Yang, M., Liu, G., et al. (2016). Proinflammatory signal suppresses proliferation and shifts macrophage metabolism from Myc-dependent to HIF1α-dependent. Proceedings of the National Academy of Sciences of the United States of America *113*, 1564–1569. https://doi.org/10.1073/pnas.1518000113.

25. Yabaji, S.M., Zhernovkov, V., Araveti, P.B., Lata, S., Rukhlenko, O.S., Abdullatif, S.A., Vanvalkenburg, A., Alekseev, Y., Ma, Q., Dayama, G., et al. (2024). Lipid Peroxidation and Type I Interferon Coupling Fuels Pathogenic Macrophage Activation Causing Tuberculosis Susceptibility. bioRxiv, 2024.03.05.583602. https://doi.org/10.1101/2024.03.05.583602.

26. Pelengaris, S., Khan, M., and Evan, G. (2002). c-MYC: more than just a matter of life and death. Nat. Rev. Cancer *2*, 764–776. https://doi.org/10.1038/nrc904.

27. Dejure, F.R., and Eilers, M. (2017). MYC and tumor metabolism: chicken and egg. EMBO J. *36*, 3409–3420. https://doi.org/10.15252/embj.201796438.

28. Casey, S.C., Baylot, V., and Felsher, D.W. (2017). MYC: Master Regulator of Immune Privilege. Trends in immunology *38*, 298–305. https://doi.org/10.1016/j.it.2017.01.002.

29. Das, S.K., Lewis, B.A., and Levens, D. (2023). MYC: a complex problem. Trends Cell Biol. *33*, 235–246. https://doi.org/10.1016/j.tcb.2022.07.006.

30. Jha, R.K., Kouzine, F., and Levens, D. (2023). MYC function and regulation in physiological perspective. Front. Cell Dev. Biol. *11*, 1268275. https://doi.org/10.3389/fcell.2023.1268275.

31. Pelengaris, S., and Khan, M. (2003). The many faces of c-MYC. Arch. Biochem. Biophys. *416*, 129–136. https://doi.org/10.1016/s0003-9861(03)00294-7.

32. Riggelen, J. van, Yetil, A., and Felsher, D.W. (2010). MYC as a regulator of ribosome biogenesis and protein synthesis. Nat. Rev. Cancer *10*, 301–309. https://doi.org/10.1038/nrc2819.

33. Pello, O.M., Pizzol, M.D., Mirolo, M., Soucek, L., Zammataro, L., Amabile, A., Doni, A., Nebuloni, M., Swigart, L.B., Evan, G.I., et al. (2012). Role of c-MYC in alternative activation of human macrophages and tumor-associated macrophage biology. Blood *119*, 411–421. https://doi.org/10.1182/blood-2011-02-339911.

34. Luiz, J.P.M., Toller-Kawahisa, J.E., Viacava, P.R., Nascimento, D.C., Pereira, P.T., Saraiva, A.L., Prado, D.S., Bert, M.L., Giurisato, E., Tournier, C., et al. (2020). MEK5/ERK5 signaling mediates IL-4-induced M2 macrophage differentiation through regulation of c-Myc expression. J. Leucoc. Biol. *108*, 1215–1223. https://doi.org/10.1002/jlb.1ma0520-016r.

35. Pello, O.M. (2016). Macrophages and c-Myc cross paths. OncoImmunology *5*, e1151991. https://doi.org/10.1080/2162402x.2016.1151991.

36. Beaulieu, M.-E., Jauset, T., Massó-Vallés, D., Martínez-Martín, S., Rahl, P., Maltais, L., Zacarias-Fluck, M.F., Casacuberta-Serra, S., Pozo, E.S.D., Fiore, C., et al. (2019). Intrinsic cell-penetrating activity propels Omomyc from proof of concept to viable anti-MYC therapy. Science translational medicine *11*, eaar5012. https://doi.org/10.1126/scitranslmed.aar5012.

37. Bowen, H., Biggs, T.E., Phillips, E., Baker, S.T., Perry, V.H., Mann, D.A., and Barton, C.H. (2002). c-Myc Represses and Miz-1 Activates the Murine Natural Resistance-associated Protein 1 Promoter*. J. Biol. Chem. *277*, 34997–35006. https://doi.org/10.1074/jbc.m204232200.

38. Wu, J., Luo, F.-L., Xie, Y., Xiong, H., Gao, Y., Liu, G., and Zhang, X.-L. (2022). EST12 regulates Myc expression and enhances anti-mycobacterial inflammatory response via RACK1-JNK-AP1-Myc immune pathway. Front. Immunol. *13*, 943174. https://doi.org/10.3389/fimmu.2022.943174.

39. Bae, S., Park, P.S.U., Lee, Y., Mun, S.H., Giannopoulou, E., Fujii, T., Lee, K.P., Violante, S.N., Cross, J.R., and Park-Min, K.-H. (2021). MYC-mediated early glycolysis negatively regulates proinflammatory

responses by controlling IRF4 in inflammatory macrophages. Cell Reports *35*, 109264. https://doi.org/10.1016/j.celrep.2021.109264.

40. Pagán, A.J., Lee, L.J., Edwards-Hicks, J., Moens, C.B., Tobin, D.M., Busch-Nentwich, E.M., Pearce, E.L., and Ramakrishnan, L. (2022). mTOR-regulated mitochondrial metabolism limits mycobacterium-induced cytotoxicity. Cell *185*, 3720-3738.e13. https://doi.org/10.1016/j.cell.2022.08.018.

41. Herrtwich, L., Nanda, I., Evangelou, K., Nikolova, T., Horn, V., Sagar, Erny, D., Stefanowski, J., Rogell, L., Klein, C., et al. (2016). DNA Damage Signaling Instructs Polyploid Macrophage Fate in Granulomas. Cell *167*, 1264-1280.e18. https://doi.org/10.1016/j.cell.2016.09.054.

42. Al-Zeer, M.A., Xavier, A., Lubad, M.A., Sigulla, J., Kessler, M., Hurwitz, R., and Meyer, T.F. (2017). Chlamydia trachomatis Prevents Apoptosis Via Activation of PDPK1-MYC and Enhanced Mitochondrial Binding of Hexokinase II. EBioMedicine *23*, 100–110. https://doi.org/10.1016/j.ebiom.2017.08.005.

43. Rajeeve, K., Vollmuth, N., Janaki-Raman, S., Wulff, T.F., Baluapuri, A., Dejure, F.R., Huber, C., Fink, J., Schmalhofer, M., Schmitz, W., et al. (2020). Reprogramming of host glutamine metabolism during Chlamydia trachomatis infection and its key role in peptidoglycan synthesis. Nat. Microbiol. *5*, 1390–1402. https://doi.org/10.1038/s41564-020-0762-5.

44. Vollmuth, N., Schlicker, L., Guo, Y., Hovhannisyan, P., Janaki-Raman, S., Kurmasheva, N., Schmitz, W., Schulze, A., Stelzner, K., Rajeeve, K., et al. (2022). c-Myc plays a key role in IFN-γ-induced persistence of Chlamydia trachomatis. Elife *11*, e76721. https://doi.org/10.7554/elife.76721.

45. Ye, Z., Petrof, E.O., Boone, D., Claud, E.C., and Sun, J. (2007). Salmonella Effector AvrA Regulation of Colonic Epithelial Cell Inflammation by Deubiquitination. Am. J. Pathol. *171*, 882–892. https://doi.org/10.2353/ajpath.2007.070220.

46. Colineau, L., Lambertz, U., Fornes, O., Wasserman, W.W., and Reiner, N.E. (2018). c-Myc is a novel Leishmania virulence factor by proxy that targets the host miRNA system and is essential for survival in human macrophages. J. Biol. Chem. *293*, 12805–12819. https://doi.org/10.1074/jbc.ra118.002462.

47. Jones, R.G., and Pearce, E.J. (2017). MenTORing Immunity: mTOR Signaling in the Development and Function of Tissue-Resident Immune Cells. Immunity *46*, 730–742. https://doi.org/10.1016/j.immuni.2017.04.028.

48. Cheng, S.-C., Quintin, J., Cramer, R.A., Shepardson, K.M., Saeed, S., Kumar, V., Giamarellos-Bourboulis, E.J., Martens, J.H.A., Rao, N.A., Aghajanirefah, A., et al. (2014). mTOR- and HIF-1α-mediated aerobic glycolysis as metabolic basis for trained immunity. Science *345*, 1250684–1250684. https://doi.org/10.1126/science.1250684.

49. Kim, J.H., Lee, S.-R., Li, L.-H., Park, H.-J., Park, J.-H., Lee, K.Y., Kim, M.-K., Shin, B.A., and Choi, S.-Y. (2011). High Cleavage Efficiency of a 2A Peptide Derived from Porcine Teschovirus-1 in Human Cell Lines, Zebrafish and Mice. PLoS ONE *6*, e18556. https://doi.org/10.1371/journal.pone.0018556.

50. Amend, S.R., Valkenburg, K.C., and Pienta, K.J. (2016). Murine Hind Limb Long Bone Dissection and Bone Marrow Isolation. J. Vis. Exp. : JoVE, 53936. https://doi.org/10.3791/53936.

51. Wilkinson, A.C., Ishida, R., Kikuchi, M., Sudo, K., Morita, M., Crisostomo, R.V., Yamamoto, R., Loh, K.M., Nakamura, Y., Watanabe, M., et al. (2019). Long-term ex vivo haematopoietic-stem-cell expansion allows nonconditioned transplantation. Nature *571*, 117–121. https://doi.org/10.1038/s41586-019-1244-x.

52. Das, A.T., Tenenbaum, L., and Berkhout, B. (2016). Tet-On Systems For Doxycycline-inducible Gene Expression. Current gene therapy *16*, 156–167. https://doi.org/10.2174/1566523216666160524144041.

53. Soucek, L., Helmer-Citterich, M., Sacco, A., Jucker, R., Cesareni, G., and Nasi, S. (1998). Design and properties of a Myc derivative that efficiently homodimerizes. Oncogene *17*, 2463–2472. https://doi.org/10.1038/sj.onc.1202199.

54. Whitfield, J.R., Beaulieu, M.-E., and Soucek, L. (2017). Strategies to Inhibit Myc and Their Clinical Applicability. Frontiers in Cell and Developmental Biology *5*, 5943–13. https://doi.org/10.3389/fcell.2017.00010.

55. Pertel, T., Reinhard, C., and Luban, J. (2011). Vpx rescues HIV-1 transduction of dendritic cells from the antiviral state established by type 1 interferon. Retrovirology *8*, 49–49. https://doi.org/10.1186/1742-4690-8-49.

56. Bankhead, P., Loughrey, M.B., Fernández, J.A., Dombrowski, Y., McArt, D.G., Dunne, P.D., McQuaid, S., Gray, R.T., Murray, L.J., Coleman, H.G., et al. (2017). QuPath: Open source software for digital pathology image analysis. Sci. Rep. *7*, 16878. https://doi.org/10.1038/s41598-017-17204-5.

Supplementary Materials

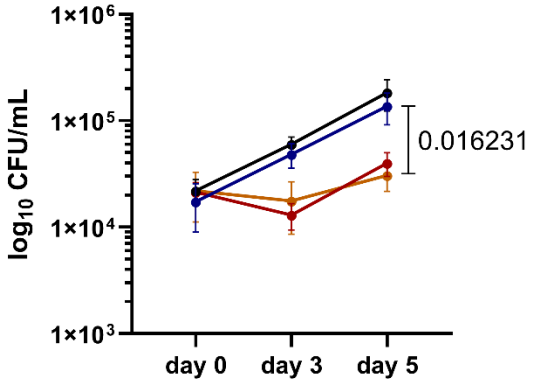

Supplementary Figure 1. IFN-γ activation of BMDMs before infection improves control of MTB growth

Quantification in colony forming units per milliliter (CFU/mL) of intracellular MTB after IFN-γ activation at different timepoints. Measurements were taken immediately after phagocytosis (day 0) and at 3 and 5 days post-infection. Data of one experiment is shown. *P* values were calculated with Student's t-test between BMDMs activated with IFN-γ before and after infection.

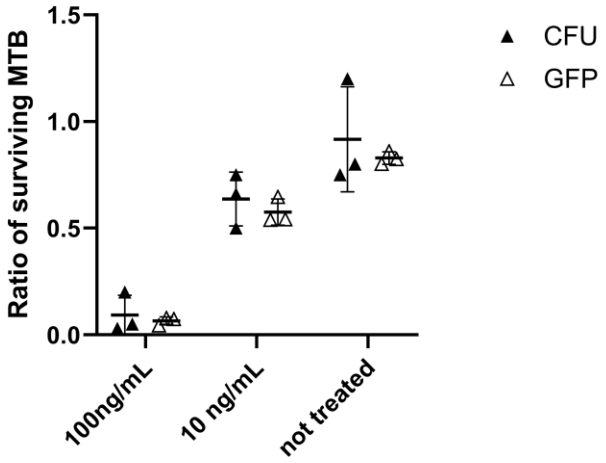

Supplementary Figure 2. Validation of MTB survival analysis using flow cytometry and CFU assays

To validate the GFP-based flow cytometry assay against the colony forming unit (CFU) assay, we infected 50'000 BMDMs per sample with the MTB live-dead strain at a multiplicity of infection (MOI) of 5. Cells were incubated for 24h, followed by activation with doxycycline for an additional 24h. Subsequently, one half of the

cell samples were lysed for CFU quantification, while the remaining cells were analyzed for GFP^{+} infected cells by flow cytometry. CFU ratios, comparing counts at baseline to those at the specified time point, were plotted to assess bacterial survival and for comparison with the MTB live-dead strain. To establish a baseline, BMDMs infected with doxycycline-preactivated live-dead bacteria (MOI 5) were immediately subjected to either CFU or flow cytometry analysis post-infection. MTB survival was assessed by exposing infected cells to varying concentrations of the antimycobacterial drug isoniazid (100 ng/mL, 10 ng/mL, and no antibiotic), providing a range of survival percentages for comparative analysis.

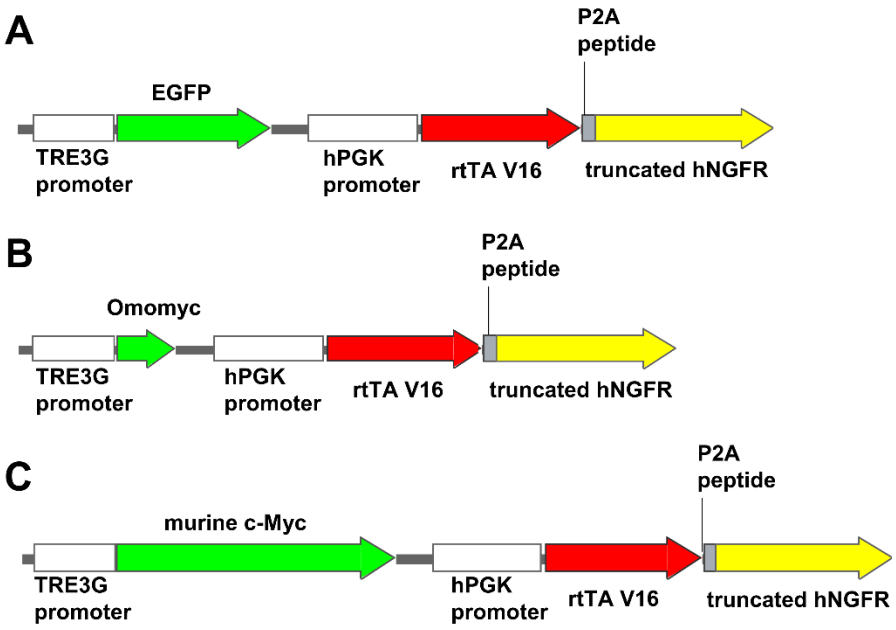

Supplementary Figure 3. Structure of lentiviral constructs containing the Tet-on system

Structure of the Tet-on constructs expressing different genes: **A)** enhanced green fluorescent protein (EGFP) **B)** Omomyc. **C)** murine c-Myc. The Human phosphoglycerate kinase 1 promoter (hPGK) is constitutively active in most human and mouse cell types. It regulates the transcription of the rTTAV16-P2A-NGFR construct. rtTAV16 is an improved version of reverse tetracycline-controlled transactivator effective at low doses of doxycyline (100ng/mL). Truncated human Nerve Growth Factor Receptor (NGFR) is the extracellular domain of the human NGFR, used in this study as marker of transduction. Porcine teschovirus 2A peptide (P2A) is a self-cleaving peptide that allows the production of two separate proteins from one transcript[49].

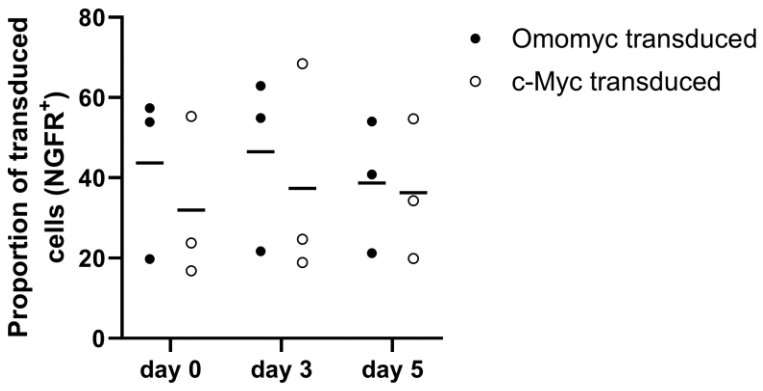

Supplementary Figure 4. Transduction rates of BMDMs across experiments

Scatter plot showing the proportion of successfully transduced BMDMs, determined by the percentage of NGFR$^+$ cells identified via flow cytometry. BMDMs were lentivirally transduced with either Omomyc or c-Myc. Each data point represents the mean percentage of NGFR$^+$ cells from an independent experiment over the different time points.

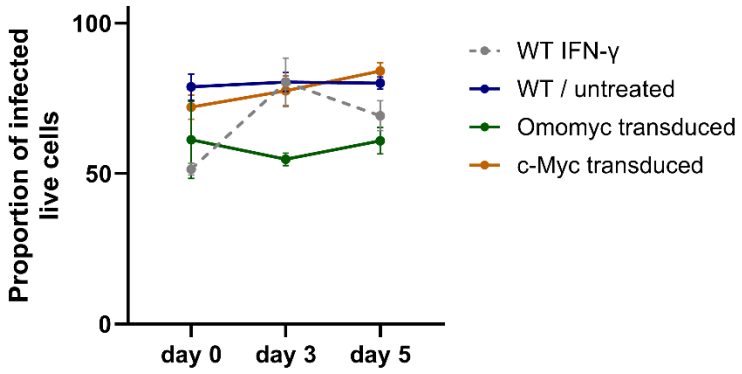

Supplementary Figure 5. Macrophage viability remains unaffected by Omomyv-mediated c-Myc inhibition over time

Proportion of live cells among infected macrophages in either wildtype, c-Myc-expressing, Omomyc-expressing, or wildtype BMDMs treated with IFN-γ (20ng/mL). Cells expressing c-Myc or Omomyc were pre-treated with 100ng/mL doxycycline for 24h before infection. IFN-γ was added from 24h before infection to the measured timepoint. The percentage of live cells was measured immediately after phagocytosis (day 0), at day 3 and 5 post-infection.

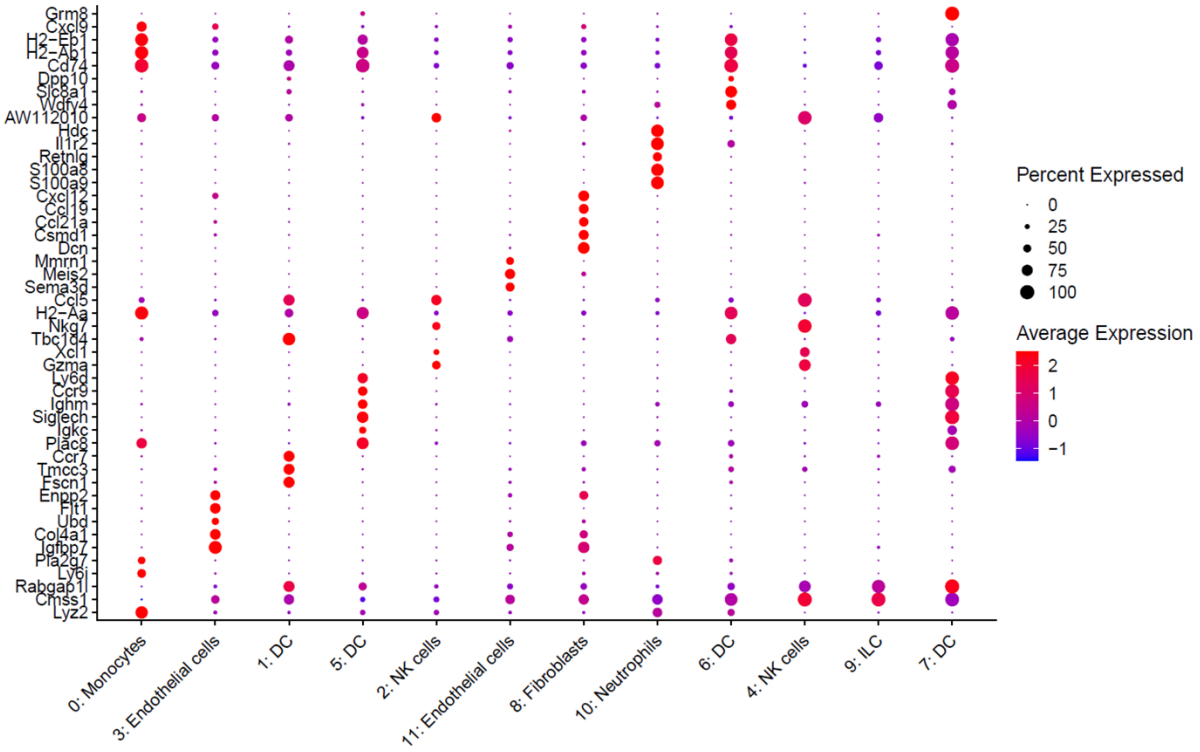

Supplementary Figure 6. Cluster-defining genes in scRNA-seq

Cluster-defining genes were used to deconvolute scRNA-seq data and generate clusters using the Seurat package[23].

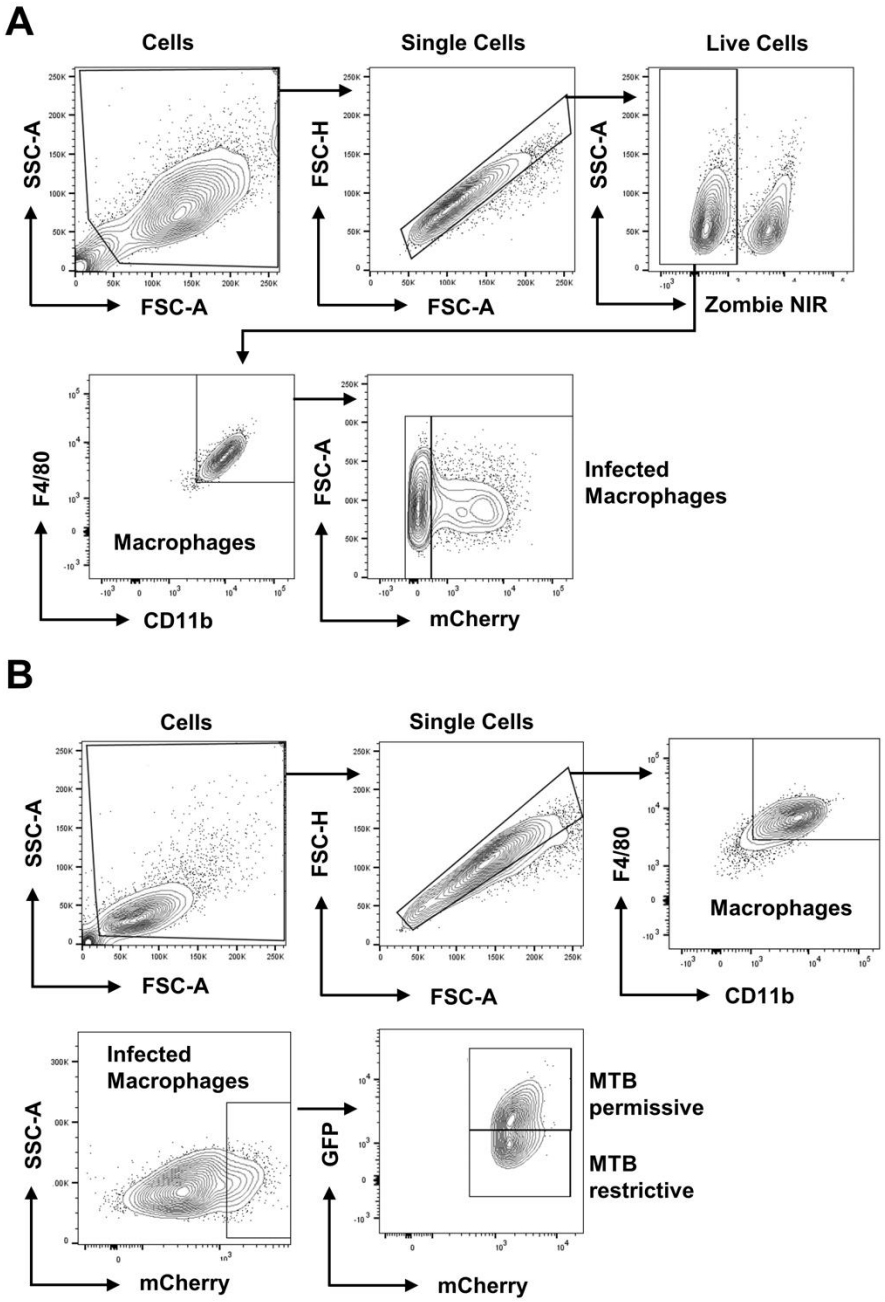

Supplementary Figure 7. Gating strategy

Flow cytometry gating strategy of infected BMDMs infected with MTB. **A)** Gating strategy for infection with mCherry-expressing MTB. **B)** Flow cytometry gating strategy for infection with MTB live-dead reporter strain.

Supplementary Table 1. Patient characteristics

	Sex	Age	Diagnosis	Mode of diagnosis
1	female	38	Retroperitoneal tuberculosis	PCR positive
2	male	21	Lymph node tuberculosis	Culture, PCR positive
3	male	73	Lymph node tuberculosis	PCR positive
4	female	28	Pleural tuberculosis	Culture positive
5	male	42	Lymph node tuberculosis	Culture positive
6	male	22	Lymph node tuberculosis	Culture positive
7	male	58	Laryngeal tuberculosis	Culture, PCR positive